



Aaron Moscho

*Candidate*

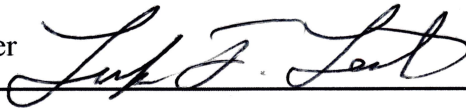
Electrical and Computer Engineering

*Department*

This thesis is approved, and it is acceptable in quality and form for publication on microfilm:

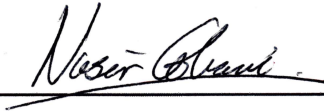
*Approved by the Thesis Committee:*

Dr. Luke F. Lester

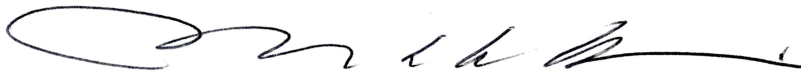


, Chairperson

Dr. Nasir Ghani



Dr. Mansoor Sheik-Bahae



Accepted:

*Dean, Graduate School*

*Date*

**INJECTION LOCKING CHARACTERISTICS OF  
INDIUM ARSENIDE QUANTUM DASH LASERS**

**BY**

**AARON MOSCHO**

**B.S., PHYSICS  
UNIVERSITY OF WISCONSIN, EAU CLAIRE**

**THESIS**

Submitted in Partial Fulfillment of the  
Requirements for the Degree of

**Master of Science**

**Electrical Engineering**

The University of New Mexico  
Albuquerque, New Mexico

**December, 2007**

## ACKNOWLEDGMENTS

I thank and acknowledge Prof. Luke F. Lester, my advisor, teacher, and dissertation chair, for continuing to encourage me through the years of classroom teachings, research guidance, and one on one discussion. His guidance and professional style will remain with me as I continue on in my career.

I also thank my committee members, Dr. Nasir Ghani and Dr. Mansoor Sheik-Bahae for their recommendations pertaining to this study, and assistance in my professional development. Gratitude is extended to the Air Force Research Laboratory, for the funding to pursue this research.

To Vassilios Kovanis, Mr. Mike Fanto, Mr. Yan Li, and Mr. Nader Nadari for their helpful discussions, comments, and guidance.

And finally I would like to thank Urivon, Darcy, and Norman for their great support and love throughout my entire educational career.

**INJECTION LOCKING CHARACTERISTICS OF  
INDIUM ARSENIDE QUANTUM DASH LASERS**

**BY**

**AARON MOSCHO**

**ABSTRACT OF THESIS**

Submitted in Partial Fulfillment of the  
Requirements for the Degree of

**Master of Science**

**Electrical Engineering**

The University of New Mexico  
Albuquerque, New Mexico

**December, 2007**

# **Injection Locking Characteristics of Indium Arsenide Quantum Dash Lasers**

**By**

**Aaron Moscho**

**B.S., Physics, University of Wisconsin, Eau Claire, 2005**

**M.S., Electrical Engineering, University of New Mexico, 2007**

## **ABSTRACT**

The study of injection locking characteristics was performed on an InAs Quantum Dash (QDash) semiconductor laser for the first time. The linewidth enhancement factor ( $\alpha$ -parameter) of a QDash laser was measured using an injection locking technique that takes advantage of the asymmetry of the injection range. Studies were performed as functions of injected photon density, wavelength, and output power. To understand the behavior of the  $\alpha$ -parameter versus wavelength, the Hakki-Paoli method, a technique that utilized the below threshold amplified spontaneous emission spectrum, was used to measure the modal gain over 1550 nm to 1573 nm.

The  $\alpha$ -parameter was found to have changed dramatically with power, indicating a large nonlinear gain coefficient,  $\epsilon$ . Using a curve fit of the  $\alpha$  versus power curve taken

from the injection locking data,  $\varepsilon$  was measured to be  $1.4 \cdot 10^{-14} \text{ cm}^3$ , 1000 times larger than the typical  $\varepsilon$  of quantum well lasers, changing the dynamics of the laser.

The small  $\alpha$ -parameter and giant  $\varepsilon$  dramatically change the dynamics of the laser. To study the effects of the small  $\alpha$ -parameter and giant  $\varepsilon$  further, an operational map was created using an Agilent Technologies High Resolution Spectrometer (HRS) with a resolution of 1 MHz. The new operational map of the InAs QDash laser has features never before seen with other devices, such as the avoidance of coherence collapse with optical feedback.

## **TABLE OF CONTENTS**

<b>LIST OF FIGURES.....</b>	<b>x</b>
<b>CHAPTER 1 INTRODUCTION .....</b>	<b>1</b>
1.1 Basic Operation of Optical Injection Locking .....	1
1.2 Injection Locking History and Previous Experiments .....	3
1.3 Applications.....	4
1.4 Quantum Dots and Dashes .....	6
1.4.1 A Brief History of the Semiconductor Laser .....	6
1.4.2 Formation of Quantum Dashes .....	6
1.4.3 Advantage of Quantum Dashes and Dots.....	7
1.5 Thesis Organization .....	11
1.6 References .....	12
<b>CHAPTER 2 LINEWIDTH ENHANCEMENT FACTOR OF AN InAs QUANTUM DASH LASER .....</b>	<b>16</b>
2.1 Device Structure .....	16
2.2 Experimental Setup.....	19
2.3 Linewidth Enhancement Factor.....	22



2.4	Injection Locking Technique.....	24
2.5	Wavelength and Power Dependence of the $\alpha$ -Parameter .....	27
2.6	ASE/Hakki Paoli Method.....	31
2.7	Conclusion.....	35
2.8	References .....	36
<b>CHAPTER 3 NONLINEAR GAIN COEFFICIENT AND OPERATIONAL MAP OF AN INAS QUANTUM DASH LASER.....</b>		<b>38</b>
3.1	Nonlinear Gain Coefficient .....	39
3.2	Relation of the Nonlinear Gain Coefficient and $\alpha$ -Parameter .....	41
3.3	Calculaton of the Nonlinear gain Coefficient.....	42
3.4	Experimental Setup.....	45
3.5	Measuring the Operational Map of an InAs Quantum Dash Injection Locked Laser .....	48
3.6	Spectrum .....	52
3.7	Zero Detuning.....	56
3.8	Conclusion.....	59
3.9	References .....	60

<b>CHAPTER 4 CONCLUDING REMARKS AND FUTURE WORK .....</b>	<b>62</b>
4.1 Concluding Remarks.....	62
4.2 Future Work .....	64

## LIST OF FIGURES

Figure 1.1 Optical injection-locking schematic .....	2
Figure 1.2 Atomic force micrograph of the InAs quantum dashes .....	7
Figure 1.3 Density of states functions for Bulk, Quantum Well, Quantum Wire, and Quantum Dot material .....	9
Figure 2.1 Schematic of the laser structure showing 5 stacks of InAs dashes imbedded in in an $\text{Al}_{0.20}\text{Ga}_{0.16}\text{In}_{0.64}\text{As}$ quantum well .....	18
Figure 2.2 Schematic of the injection-locking setup .....	21
Figure 2.3 Optical spectra of the injection locked laser at a dominant FP mode (top) and the free-running slave (bottom) biased at 70 mA with a peak wavelength $\sim 1567$ nm ...	26
Figure 2.4 Optical spectra of the injection locked laser at a weak side mode at 1550 nm and the free running slave biased at 70 mA with a peak wavelength $\sim 1565$ nm .....	29
Figure 2.5 Plot of $\alpha$ vs. current above threshold. The $\alpha$ -parameter has a strong relation to the output power of the slave laser, indicating a large nonlinear gain coefficient .....	30
Figure 2.6 Measurement of the ASE at 44 mA (1 mA below threshold) showing the peaks marked in red, and valleys marked in blue .....	33
Figure 2.7 Net modal gain spectra calculated from the ASE spectrum .....	34
Figure 3.1 The $\alpha$ -parameter versus output power of the slave laser .....	44
Figure 3.2 Schematic of experimental setup used for measuring the operational map ...	47
Figure 3.3 Operational map of an InAs Quantum Dash injection locked laser .....	50
Figure 3.4 A side by side comparison of an operational make made by a conventional edge-emitting semiconductor laser and an InAs quantum dash edge-emitting laser .....	51
Figure 3.5 Spectrum of a) Unlocked, b) Stable Locked, c) Period 1 d) Period Doubling, e) four wave mixing, f) Coherence Collapse .....	55
Figure 3.6 Spectra of InAs Quantum Dash laser injection locked at zero detuning .....	58

## Chapter 1: Introduction

Over the past 30 years, the field of digital and analog transmission of data over fibers has driven the telecommunications field. This data transmission capability has led to many important applications, most notably long distance and trans-Atlantic communications. The addition of wavelength-division multiplexing (WDM) in the early 1990s, where multiple transmitter wavelength channels are transmitted in a single fiber, has dramatically increased the bandwidth of communication systems.

Directly-modulated semiconductor lasers are the most compact sources for these telecommunication systems; however, their applications have been limited to relatively low frequencies of 10 Gb/s because of small relaxation oscillations and high chirp. Because of this, new transmitters are needed to be able to increase the bandwidth of fiber-optic communication systems. Implementing injection-locked semiconductor lasers into these systems has proven to be a way of improving the bandwidth and performance of these systems.

### 1.1 Basic Operation of Optical Injection Locking

The optical injection-locking technique for semiconductor lasers consists of two optical sources referred to as the master and slave (also called “follower”) lasers. The master laser, typically a high-power narrow-linewidth tunable laser, is injected into the slave laser, thereby affecting the operation and behavior of the slave laser as shown in figure 1.1. When the two frequencies are nearly matched, the phase locking phenomenon

occurs, and properties of the injection-locked output, such as a suppression of the side modes, become evident.

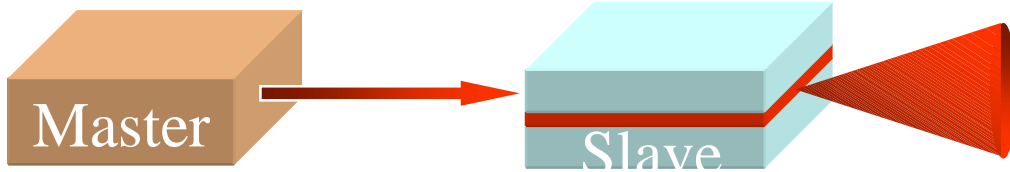


Figure 1.1) Optical injection-locking schematic

Two important control-parameters of an injection-locked semiconductor laser system are the frequency detuning,  $Df$ , and injection ratio,  $h$ . The frequency detuning is the difference in frequency of the master and the free-running slave laser Fabry-Perot (FP) mode, so that  $Df = f_{slave} - f_{master}$ . The injection ratio is defined as the ratio of the injected optical power from the master into the slave cavity over the power of the slave laser right outside of the slave's cavity,  $h = \frac{P_{master}}{P_{slave}}$ , where  $P_{master}$  and  $P_{slave}$  are the output powers of the master and slave, respectively.

Under operation, the injection-locking system can be in one of six unique states depending on the frequency detuning and injection ratio: unlocked, stably locked, four-wave mixing, relaxation oscillations (also termed "period one"), period doubling (also termed "period two"), or coherence collapse. In the stably locked and period one regions, injection-locked semiconductor lasers can outperform direct-modulated transmitters due to their lower laser noise, non-linearities, low chirp, and narrow linewidth. The coherence collapse state is an undesirable state in most situations where the linewidth

suddenly broadens severely, up to  $\sim 10$  GHz. A further discussion of these injection-locked states and spectra will be presented in chapter three of this thesis. By using the injection locking technique, the linewidth of a multi-mode FP laser can be reduced from its free running linewidth of  $\sim 100$  GHz to as low as the narrow linewidth of the master laser,  $\sim 100$  kHz. Because the frequency of the system is locked at a certain value, the chirp is dramatically reduced, and since the other modes of the FP cavity are suppressed, mode-hopping is also suppressed.

## 1.2 Injection-Locking History and Previous Experiments

The locking phenomenon between two oscillators has been an area of interest for scientist and mathematicians since the 1600's when Huygens observed synchronization between two pendulum clocks on a wall<sup>1</sup>. This phenomenon was relatively unknown until R. Adler established a theoretical study on locking phenomena in electric oscillators in 1946<sup>2</sup>. In 1966, the theory of locking phenomenon was applied to optical oscillators when Stover and Steier demonstrated the first case of injection locking when they locked two HeNe lasers<sup>3</sup>.

When well-engineered AlGaAs semiconductor lasers became available in the 1980s, injection-locking of semiconductor lasers were studied and proposed for applications in coherent optical communication<sup>4</sup> as a method to reduce laser noise and optical linewidth of the laser. Also during the 1980's, Kobayashi *et al.* demonstrated stable single-mode operation of Fabry-Perot lasers<sup>5</sup>, and phase modulation of an injection locked laser<sup>6</sup> using AlGaAs lasers. During these pioneering days of injection locking

semiconductor lasers, the work was focused on the weak injection regime<sup>7</sup>. In this regime, the locking range is typically very small. Additionally, this regime exhibits chaotic behavior, resonant oscillations, and an unstable locking range that hinders the usefulness of injection locking in practical systems<sup>8</sup>.

Since the 1990s, many advances have been made in injection-locked lasers including reduced chirp<sup>9</sup> and linewidth, improved modulation bandwidth enhancement<sup>10</sup>, increased resonance frequency<sup>11</sup>, smaller nonlinear distortion<sup>12</sup>, and lower relative intensity noise<sup>13</sup>. In 2000, Lee *et al.* showed bandwidth enhancement to 28 GHz and a reduction in chirp using a 1.55- $\mu\text{m}$  distributed feedback (DFB) laser<sup>14</sup> as the slave device. Injection-locking of a 1.55  $\mu\text{m}$  vertical cavity surface emitting laser (VCSEL) was demonstrated for the first time in 2003 by Cheng *et al.*<sup>15,16</sup>.

### 1.3 Applications

Recently, the injection-locking technique has been used in several applications including radio-over-fiber<sup>20</sup> and millimeter-wave generation<sup>21</sup>, and all-optical signal processing<sup>22</sup>.

The transmission of analog and digital signals over high-frequency carriers, with frequencies around a few tens of GHz, through optical fibers has attracted great interest in the last few years, since optical fibers have very low propagation loss of about 0.2 dB/km around 1.55  $\mu\text{m}$ . For Radio over Fiber (ROF) systems, millimeter (mm) wave signals are generated using optical sources, and transmitted through fibers. Goldberg, Yurek, Taylor, and Weller first demonstrated this technique by injection

locking two longitudinal modes of two independent optical sources (slave lasers) to two FM sidebands of the master laser<sup>23</sup>.

Using this mm carrier generated by sideband injection locking, reports of 155 Mb/s data transmission on a carrier of 64 GHz over 12.8 km have been demonstrated using a standard single-mode fiber<sup>24</sup>.

A simpler technique demonstrated by Noel *et al.*, which only used one master laser and one radio frequency (RF) modulated slave laser, has demonstrated to generate high-purity tunable millimeter waves<sup>25</sup>. Recently, injection locking for millimeter wave generation has been extended to using passively mode-locked DBR lasers<sup>26</sup> and two section DFB lasers<sup>27</sup>.

All optical signal processing can lighten the requirements of electric circuits in high-speed photonic networks. Clock recovery, which is essential to digital communication, can be achieved by injection locking a passively mode-locked laser<sup>28</sup>, injection locked DFB Laser<sup>29,30</sup>, and a two-mode injection locked FP laser<sup>31</sup>.

All optical signal processing is based on the switching of locking stability as a function of the injection ratio. By fixing the frequency detuning, the locked and unlocked states depends on the injection power. When the optical power is higher than the locking threshold, the slave laser is locked to the master laser's frequency. If the injection power is lower than the locking threshold, the slave laser operates at its original frequency. Due to the threshold behavior of the locking and unlocking processes, distorted signals can be reshaped, resulting in a frequency-modulated signal with reduced noise. The signal generated by the slave laser can then be filtered, so the regenerated signal can be obtained.



## 1.4 Quantum Dots and Dashes

### *1.4.1 A brief history of the semiconductor laser*

In 1962, R.N. Hall developed and demonstrated the first working semiconductor laser<sup>36</sup>. Although a breakthrough in science, this simple pn homojunction laser suffered from small efficiencies and large threshold currents. A year later, H. Kroemer proposed the principle of a double heterostructure (DH) laser. From the concept in 1963, the first continuously operating (CW) laser was demonstrated in 1970 using a lattice-matched AlGaAs/GaAs DH laser structure<sup>37</sup>.

An improvement to the DH laser was made in the late 1970's when the active region was reduced to the order of the de Broglie wavelength, into a quantum well (QW). In QW lasers, the carriers are confined within quantized energy levels due to the small volume of the material, thereby allowing control over the wavelength by adjusting the thickness of the well. The benefits of the one dimensional confinement of the quantum well inspired people to look for higher orders of carrier confinement. In 1982, Arakawa and Sakaki projected the next advance in the semiconductor laser, the quantum dot<sup>38</sup>. This new nanostructure was predicted to make the device less temperature dependent than other semiconductor lasers, as well as a further reduce the threshold current, and increase the differential gain and speed compared to quantum well devices.

### *1.4.2 Formation of Quantum Dashes*

InAs quantum dashes (QDash) are typically grown on InP substrates by growth techniques such as solid-source molecular beam epitaxy (MBE), gas source MBE (GS-

MBE). and metal organic vapor phase epitaxy (MOVPE). Two approaches have been developed to effectively grow InAs QDashes on InP: the first one developed used the (3 1 1)B surface, and the latter being the optimization on (1 0 0) oriented substrates.

Currently, QDashes grown on the (1 0 0) oriented substrate have become the more practiced growth technique are typically elongated along the [1 -1 0] direction. The nanostructure's self-organization in this direction can be explained by the step-edges on the oriented surface. These step-edges are terminated, therefore more reactive with indium, resulting in the growth of InAs QDashes proceeding faster in the [1 -1 0] direction<sup>39</sup>.

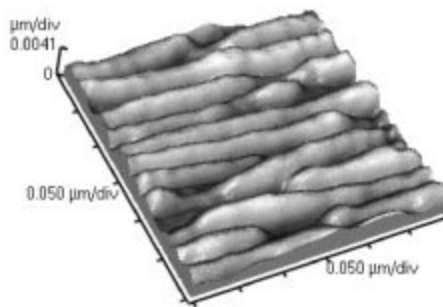


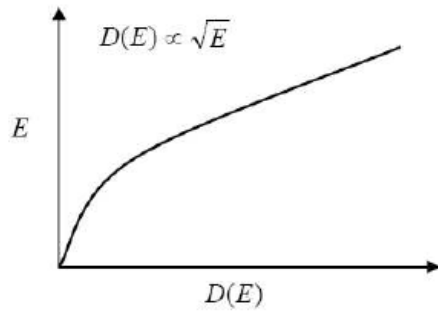
Figure 1.2) Atomic force micrograph of the InAs quantum dashes

#### ***1.4.3 Advantage of Quantum Dashes and Dots***

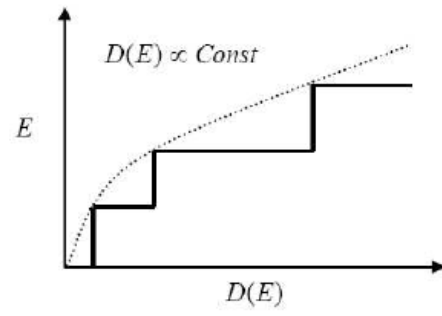
Quantum dashes, and more generally quantum dots, offer many advantages over traditional DH and QW laser diodes such as large characteristic temperatures ( $T_0$ ), low threshold current, small linewidth enhancement factor,  $\alpha$ , and resistance to optical feedback.

### ***Large Characteristic Temperatures $T_0$***

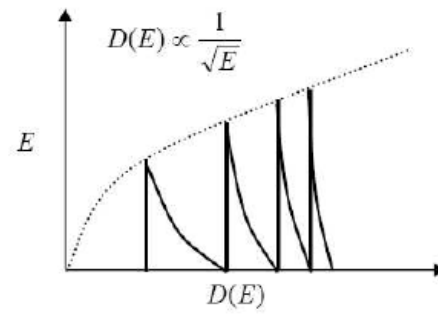
Due to the three-dimensional carrier confinement, electrons in quantum dots (QDs) show a distinct energy spectrum. This can be extended to QDash structures since, the confinement in the long dimension of QDash structures is somewhat less than in dots but still follows the general physics. Because of 3D confinement, the spacing between atomic-like states is greater than the available thermal energy present, which hinders the thermal depopulation of the lowest electronic states. This effect gives rise to a large characteristic temperature  $T_0$ <sup>40</sup>.  $T_0$  is related to the threshold current by the phenomenological relation:  $I = I_0 e^{\frac{T}{T_0}}$ , where  $I$  is the threshold current,  $I_0$  is the initial threshold current, and  $T$  is the operating temperature. Since fluctuation of the current with temperature is an undesirable effect, the high  $T_0$  of QDs makes them an attractive material structure in semiconductor lasers. Besides the inherently high  $T_0$ , it is also possible to raise  $T_0$  by optimization of p-doping<sup>41</sup> or tunnel injection<sup>42</sup>.



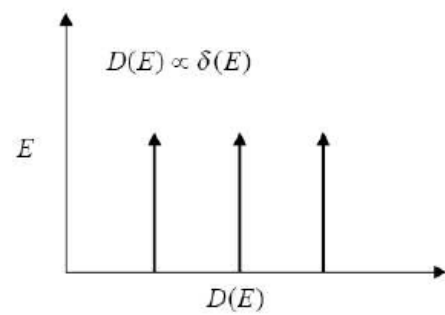
a)



b)



c)



d)

Figure 1.3) Density of states functions for a) Bulk, b) Quantum Well, c) Quantum Wire, d) Quantum Dot

### ***Low Threshold Current***

In 1982, Sakaki and Arakawa predicted that quantum dots would have a threshold current density significantly lower than quantum wells. The theory predicted that with the quantum dot's ultra-small active volume, fewer carriers would be necessary to create enough gain for lasing, hence, a low threshold current would be possible<sup>38</sup>. For QDs, threshold currents under CW operation can be as low as 10 A/cm<sup>2</sup> per layer<sup>43</sup>.

### ***Small Linewidth Enhancement Factor, $a$***

The linewidth enhancement factor,  $a$ , is an important-parameter in semiconductor lasers that impacts the linewidth, chirp, and beam-quality of the device. The  $\alpha$ -parameter is defined as the change of the real part of the refractive index as a function as the carrier density to the change of the imaginary part of the refractive index as a function of carrier density.

$$a = -\frac{dn_r/dN}{dn_i/dN} \quad (1.1)$$

Where  $N$  is carrier density,  $n_r$  is the real part of the refractive index, and  $n_i$  is the imaginary part of the refractive index<sup>44</sup>. The real and imaginary parts of the refractive index can be related by the Kramers-Kronig relation. Since the density-of-states of ideal QDs is a delta function and in practice a Gaussian shape (see Fig. 1.3), the Kramers-Kronig relation predicts that  $dn_r/dN$  is zero at the optical gain peak of a

QD ensemble. The introduction of  $\alpha$  not only explained the experimentally-observed broad linewidth and large chirp of semiconductor lasers, but also the coherence collapse due to optical feedback and filamentation in the beam of broad area lasers and amplifiers. Values for  $\alpha$  as low as 0.1 have been reported in quantum dot lasers<sup>44,45</sup>. A further discussion of the  $\alpha$ -parameter will be presented in chapter two.

### ***Resistance to Optical Feedback***

Due to many of the advantages listed above, QD lasers have become very promising as sources for communication systems. Another advantage that QD lasers have over DH and QW lasers is their strong resistance to optical feedback due to low values of the  $\alpha$ -parameter and a large relaxation oscillation damping rate, which normally leads to coherence collapse in semiconductor lasers. Coherence collapse leads to a dramatic broadening of the laser's linewidth and leads to large bit-error rates and an increase in relative intensity noise (RIN) for the laser. To reduce the feedback, an isolator is typically placed in front of the source. Since QD lasers have strong resistance to optical feedback, the isolator can be removed, decreasing the packaging cost and size of the sources for these communication systems<sup>46,47</sup>.

## 1.5 Thesis Organization

This thesis will describe the optical injection of multi-mode Fabry-Perot InAs quantum dash lasers. Chapter two presents theoretical and experimental discussions of the linewidth enhancement-parameter. Also discussed within the

chapter is the device structure of in InAs quantum dash laser, and an explanation of the experimental setup.

Chapter three focuses on nonlinear gain saturation and the nonlinear gain coefficient. The theory, effects, and calculations of the nonlinear gain coefficient are presented. Chapter three also presents the operational map of our InAs quantum dash injection-locked laser, as well as short discussions on the six unique states possible while performing our injection-locking experiments.

Chapter four is the conclusion, highlighting the most important points of this thesis. Chapter four also presents the current work, and future projects planned for injection locking of quantum dash and quantum dot semiconductor lasers.

## 1.6 References

---

<sup>1</sup> A. Pikovsky, M. Rosenblum, J. Kurths "Synchronization: A Universal Concept in Nonlinear Science" Cambridge University Press 2001

<sup>2</sup> R. Adler, "A study of Locking Phenomena in oscillators" Proc. IRE, vol.34, pp.351-357, 1946

<sup>3</sup> H. L. Stover and W. H. Steier, "Locking of laser oscillators by light injection," *Appl. Phys. Lett.*, vol. 8, no. 4, pp. 91-93, Feb. 1966

<sup>4</sup> Y. Yamamoto and T. Kimura "Coherent Optical fiber Transmission Systems" IEEE Journal of Quantum Electronics, vol. 17, pp 919-935, 1981

<sup>5</sup> S. Kobayashi and T. Kimura, "Optical phase modulation in an injection locked AlGaAs semiconductor laser," *IEEE Trans. Microw. Theory Tech.*, vol. 82, no. 10, pp. 1650-1657, Oct. 1982

<sup>6</sup> S. Kobayashi and T. Kimura "Injection locking characteristics of AlGaAs semiconductor laser," IEEE J. Quantum Electron. Vol 16, no. 9, pp.915-917, sep. 1980

<sup>7</sup> Mogensen, F; Olesen, H; Jacobsen, G; "Locking Conditions and Stability Properties for a Semiconductor Laser with External Light Injection," IEEE Journal of Quantum Electronics, Vol. 21, No. 7, pp. 784-793, 1985

<sup>8</sup> Sacher, J; Baums, D; Panknin, P; Elsasser, W, Gobel, E. O; "Intensity instabilities of semiconductor lasers under current modulation, external light injection, and delayed feedback," Physical Review A, Vol. 45, No. 3, pp 1893-1905, 1992

- 
- <sup>9</sup> S. Mohrdiek, H. Burkhard, and H. Walter, "Chirp reduction of directly modulated semiconductor lasers at 10 Gb/s by strong CW light injection," *J. Lightw. Technol.*, vol. 12, no. 3, pp. 418-424, Mar. 1994
- <sup>10</sup> J. Wang, M. K. Haldar, L. Li, and F. V. C. Mendis, "Enhancement of modulation bandwidth of laser diodes by injection locking," *IEEE Photon. Technol. Lett.*, vol. 8, no. 1, pp. 34-36, Jan. 1996
- <sup>11</sup> T. B. Simpson, J. M. Liu, K. F. Huang, K. Tai, C. M. Clayton, A. Gavrielides, and V. Kovanis, "Cavity enhancement of resonant frequencies in semiconductor lasers subject to optical injection," *Phys. Rev. A*, vol. 52, no. 6, pp. R4348-51, Dec. 1995
- <sup>12</sup> X. J. Meng, T. Chau, and M. C. Wu, "Improved intrinsic dynamic distortions in directly modulated semiconductor lasers by optical injection locking," *IEEE Trans. Microw. Theory Tech.*, vol. 47, no. 7, pp. 1172-1176, Jul. 1999
- <sup>13</sup> P. Spano, S. Piazzolla, and M. Tamburrini, "Frequency and intensity noise in injection locked semiconductor lasers: Theory and experiments," *IEEE J. Quantum Electron.*, vol. 22, no. 3, pp. 427-435, Mar. 1986
- <sup>14</sup> H. L. T. Lee, R. J. Ram, O. Kjebon, and R. Schatz, "Bandwidth enhancement and chirp reduction in DBR lasers by strong optical injection," *Conference on Lasers and Electro-Optics (CLEO 2000)*, pp. 99-100, May 2000
- <sup>15</sup> Chang, CH; Chrostowski, L; Chang-Hasnain, CJ, "Injection locking of VCSELs," *IEEE JOURNAL OF SELECTED TOPICS IN QUANTUM ELECTRONICS*; v.9, no.5, p.1386-1393, 2003
- <sup>16</sup> Chrostowski, L; "Optical Injection Locking of Vertical Cavity Surface Emitting Lasers," University of California at Berkeley, 2003
- <sup>20</sup> Kaszubowska, A. Anandarajah, P. Barry, L.P., "Improved performance of a hybrid radio/fiber system using a directly modulated laser transmitter with external injection" *IEEE Photonics Technology Letters*, vol. 14, pp 233-235, 2002
- <sup>21</sup> Al-Mumin, M; Wang, XH; Mao, WM; Pappert, SA; Li, GF "Optical generation and sideband injection locking of tunable 11-120GHz microwave/millimetre signals," *ELECTRONICS LETTERS*; Vol.36, No.18, p.1547-1548, 2000
- <sup>22</sup> Onishi, Y; Koyama, F; "All-optical regeneration using a vertical-cavity surface-emitting laser with external light injection," *IEICA Transactions on Electronics*, Vol. E87C, No. 3, 2004
- <sup>23</sup> Goldberg, L; Yurek, A.M, Taylor, H.F; Weller, J.F; "35 GHz microwave signal generation with an injection-locked laser diode," *Electronic Letters*, Vol. 21, pg. 814-815, 1985
- <sup>24</sup> Braun, R.P; Grosskopf, G; Rohde, D; Schmidt, F; "Low-phase-noise millimeter-wave generation at 64 GHz and data transmission using optical sideband injection locking," *IEEE Photonics Technology Letters*, Vol. 10, No. 5, 1998
- <sup>25</sup> Noel, L; Marcenac, D; Wade, D; "Optical millimeter-wave generation technique with high efficiency, purity and stability," *Electronics Letters*, Vol. 32, No. 21, 1996
- <sup>26</sup> Ahmed, Z; Liu, H.F; Novak, D, Ogawa, Y, Pelusi, M.D; Kim, D.Y; "Locking characteristics of a passively mode-locked monolithic DBR laser stabilized by optical injection," *IEEE Photonics Technology Letters*, Vol. 8, No. 1, 1996



- 
- <sup>27</sup> Jin, H; Rongqing, H; "Tunable millimeter-wave generation with subharmonic injection locking in two section strongly gain-coupled DFB lasers," IEEE Photonics Technology Letters, Vol. 12, No. 5, 2000
- <sup>28</sup> Mathason, B.K; Delfyett, P.J; "Pulsed injection locking dynamics of passively modelocked external-cavity semiconductor laser systems for all-optical clock recovery," Journal of Lightwave Technologies, Vol. 18, No. 8, 2000
- <sup>29</sup> Yamashita, S; Matsumoto, D; "Waveform reshaping based on injection locking of a distributed-feedback semiconductor laser," IEEE Photonics Technology Letters, Vol. 12, No. 10, 2000
- <sup>30</sup> Kuramoto, A; Yamashita, S; "All-optical regeneration using a side-mode injection locked semiconductor laser," IEEE Journal of Selected Topics Quantum Electronics, Vol. 9, No. 5
- <sup>31</sup> Yamashita, S; Suzuki, J; "All-optical 2R regeneration using a two-mode injection locked Fabry-Perot laser diode," IEEE Photonics Technology Letters, Vol. 16, No. 4, 2004
- <sup>36</sup> R. N. Hall, G. E. Fenner, J. D. Kingsley, T. J. Soltys, and R. O. Carlson, "Coherent Light Emission From GaAs Junctions," Physics Review Letter 9, pp. 366, 1962
- <sup>37</sup> I. Hayashi, M. B. Panish, P. W. Foy, and S. Sumski, "Junction lasers which operate continuously at room temperature" *Appl. Phys. Lett.*, vol.17, pp. 109-111, 1970
- <sup>38</sup> Sakaki, H; Arakawa, Y; Nishioka, M; Yoshino, J; Okamoto, Hi Miura, N; "Light-Emission from Zero-Dimensional Excitations- Photoluminescence from Quantum Wells in Strong Magnetic Fields" Applied Physics Letters; Vol. 46, No.1, p.83-85, 1985
- <sup>39</sup> Wang, R. H; Stintz, A; Varangis, M. M; Newell, T. C; Li, H; Malloy, K. J; Lester, L.F; "Room-Temperature Operation of InAs Quantum-Dash Lasers on InP (001)," IEEE Photonics Technology Letters, Vol. 13, No. 8, 2001
- <sup>40</sup> Liu H. Y.; Badcock T. J.; Groom K. M.; Hopkinson M.; Gutierrez M.; Childs D. T.; Jin C.; Hogg R. A.; Sellers I. R.; Mowbray D. J.; Skolnick M. S.; Beanland R.; and Robbins D. J.; "High-performance 1.3- $\mu\text{m}$  InAs/GaAs quantum-dot lasers with low threshold current and negative characteristic temperature," *Proc. SPIE Int. Soc. Opt. Eng.*, France 2006
- <sup>41</sup> Li, Y.; Rotter, T.J.; Xin, Y.; Stintz, A.; Matrinez, A.; Malloy, K.J.; Lester, L.F.; "High Characteristic temperature of p-doped InAs quantum dots-in-a-well laserson InP substrate," in Proc. Conf. Lasers Electro-Optic, 2006
- <sup>42</sup> Mi, Z.; Yang, L.; Bhattacharya, P.; "Growth and characteristics of p-doped InAs tunnel inection quantum-sash lasers on InP," IEEE Photonics Technology letters, Vol. 18, No. 9-12 p. 1377-1379
- <sup>43</sup> Lelarge, F; Dagens, B; Renaudier, J; Brenot, R; Accard, A; van Dijk, F; Make, D; Gouezigou, O. L; Provost, J. G; Poingt, F; Landreau, J; Drisse, O; Derouin, E; Rousseau, B; Pommereau, F; Duan, G. H; "Recent Advances on InAs/InP Quantum Dash Based Semiconductor Lasers and Optical Amplifiers Operating at 1.55  $\mu\text{m}$ ," IEEE Journal of Selected Topics in Quantum Electronics, Vol. 13, No. 1, 2007
- <sup>44</sup> Newell, T.C; Bossert, D.J; Stintz, A; Fuchs, B; Malloy, K.J; Lester, L.F; "Gain and linewidth enhancement factor in InAs quantum-dot laser diodes," IEEE Photonics Technology Letters, Vol. 11, No. 12, 1999
- <sup>45</sup> Qasaimeh, O; "Linewidth enhancement factor of quantum dot lasers," Optical and Quantum Electronics Vol. 37, No.5, pp.495-507, 2005

---

<sup>46</sup> Su, H; Zhang, L; Gray, A.L; Wang, R; Newell, T.C; Malloy, K.J; Lester, L.F; "High external feedback resistance of laterally loss-coupled distributed feedback quantum dot semiconductor lasers," IEEE Photonics Technology Letters, Vol. 15, No. 11, 2003

<sup>47</sup> O'Brien, D; Hegarty, S.P; Huyet, G; McInerney, J.G; Kettler, T; Laemmlin, M; Bimberg, D; Ustinov, V.M; Zhukov, A.El Mikhlin, S.S; Kovsh, A.R; "Feedback sensitivity of 1.3  $\mu\text{m}$  InAs/GaAs quantum dot lasers," Electronic Letters, Vol. 39, No. 25, 2003

## Chapter 2: Linewidth Enhancement Factor of an InAs Quantum Dash Laser

The linewidth enhancement factor (also termed “ $\alpha$ -parameter”) is a property of deep interest in the dynamics and characterization of semiconductor lasers. In 1982, C. Henry introduced this amplitude-phase coupling-parameter to describe the cause of the significantly higher linewidths that were experimentally measured, but not previously theoretically predicted in semiconductor lasers.

Since the introduction of the  $\alpha$ -parameter, several techniques have been implemented for measuring its value; such as interferometer measurements<sup>1</sup>, RF-modulation<sup>2</sup>, linewidth measurement above<sup>3</sup> and below<sup>4,5</sup> the threshold current, and amplified spontaneous emission (ASE)<sup>6</sup> measurements. The  $\alpha$ -parameter can vary a significant amount, up to 30% on the same device, depending on which of these techniques are used; however, each one is valid depending on the application.<sup>7</sup>

### 2.1 Device Structure

Many advantages of quantum dot and dash materials were presented in Chapter 1, such as temperature stability, low threshold current, and low  $\alpha$ -parameter. The device investigated in these experiments is MBE-grown on an  $n^+$ -InP (0 0 1) substrate as described in Chapter 1. The dashes-in-a-well (DWELL) active region consists of 5 stacks of InAs quantum dashes embedded in compressively-strained  $\text{Al}_{0.20}\text{Ga}_{0.16}\text{In}_{0.64}\text{As}$  quantum wells separated by 30-nm undoped tensile-strained  $\text{Al}_{0.28}\text{Ga}_{0.22}\text{In}_{0.50}\text{As}$  spacers

on both sides of the DWELLS. A lattice-matched 105 nm layer of undoped  $\text{Al}_{0.30}\text{Ga}_{0.18}\text{In}_{0.52}\text{As}$  is added above and below the active region. The p-cladding  $\text{AlInAs}$  layer has a thickness of 1.5  $\mu\text{m}$  and is step-doped with beryllium to reduce the free carrier loss. The n-cladding layer is 500-nm thick  $\text{AlInAs}$ . The laser structure is capped with a 100-nm  $\text{p}^{++}\text{-InGaAs}$  layer. A schematic for the device is shown in figure 2.1.

Four-micron wide ridge waveguide multi-mode Fabry-Perot lasers with 500- $\mu\text{m}$  cleaved cavity lengths were fabricated. The slope efficiency and threshold current were measured to be 0.2 W/A and 45 mA respectively. These devices were designed, grown and processed by Zia Laser.

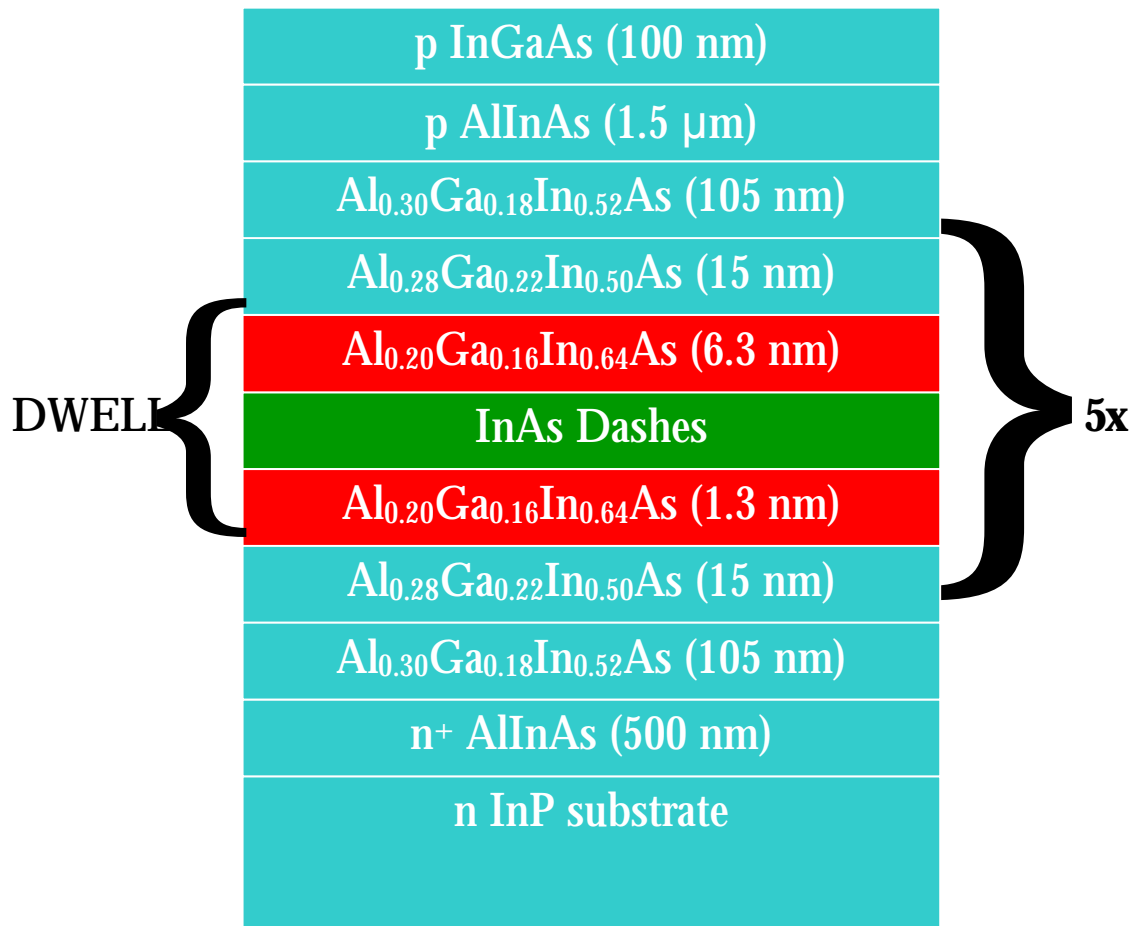


Figure 2.1) Schematic of the laser structure showing 5 stacks of InAs dashes imbedded in an Al<sub>0.20</sub>Ga<sub>0.16</sub>In<sub>0.64</sub>As quantum well.

## 2.2 Experimental Setup

A fiber-based optical injection experiment was assembled by the author and collaborators at the Sensors Directorate of the Air Force Research Laboratory in Rome, New York in the Summer of 2007. This apparatus, as shown in Figure 2.2, was used for measuring the  $\alpha$ -parameter. The first port connected into the circulator consists of a New Focus Velocity-model external cavity laser (ECL) acting as the master, with a tunable range from 1530 nm to 1580 nm and an accuracy of 4 pm. The New Focus laser is then connected to an Erbium-Doped Fiber Amplifier (EDFA) capable of 1-Watt output power, and then run through a Santec band-pass filter to decrease the noise coming from the amplified signal. From the filter a Variable Optical Attenuator (VOA) is connected which allows for greater control of the injected power into the circulator. After the VOA, a free-space polarization controller with a half-wave plate, quarter-wave plate, and linear controller is inserted to ensure polarization control of the injected field, and allowing a way to block the master laser from the polarization maintaining (PM) circulator. Port two of the circulator is coupled to the slave laser via an anti-reflection (AR) coated PM lensed fiber. The slave laser is operated at a heat sink temperature of 20 °C using a Peltier temperature controller, and biased with an ILX current source. To get maximum alignment of the slave laser, the AR-coated PM lensed fiber is mounted in a five-axis stage. Port three, the diagnostic port, has a 1x2 fiber coupler (5%/95%) in which the 5% end is connected to an ILX power meter to allow continuous monitoring of slave laser's power and alignment at port 2, while the 95% is connected to an Ando optical spectrum analyzer (OSA) with a resolution of 20 pm. This system allowed for constant monitoring

of the total power, as well as the slave power by simply blocking the master's light from going into port 1 at the polarization controller.

The  $\alpha$ -parameter measurement was conducted over a variety of wavelengths ranging from 1550 nm to 1573 nm. The limitation to the examined range when the master laser is on the shorter wavelength (blue) side came from the unstable locking of the FP slave modes, and the limitation on the longer wavelength (red) side was determined by the band pass filter. The loss from port 1 to 2 was measured to be 6 dB, and the maximum coupling efficiency of the fiber to the slave was 25%.

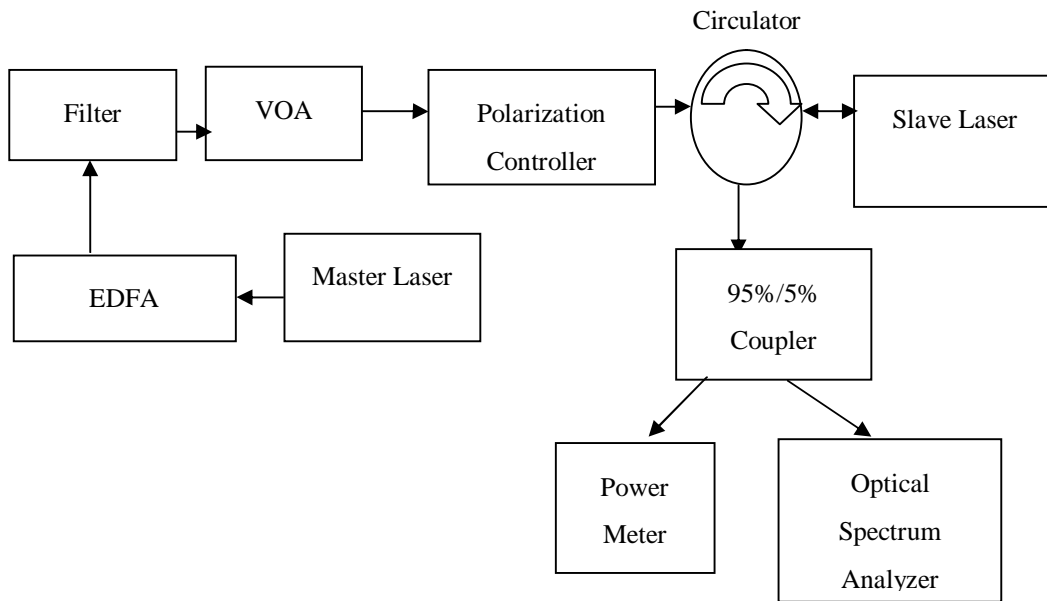


Figure 2.2) Schematic of the injection-locking setup.



### 2.3 Linewidth Enhancement Factor

As briefly described in Chapter 1, the  $\alpha$ -parameter is an important property present only in semiconductor lasers. To benefit from all of the properties a semiconductor laser has over other types of lasers, this parameter should be kept as low as possible, ideally under about 2. The  $\alpha$ -parameter resulting from the change of the real part of the refractive index as a function of the carrier density to the change of the imaginary part of the refractive index as a function as carrier density is:

$$a = \frac{dn_r/dN}{dn_i/dN} \quad (2.1)$$

Where  $N$  is carrier density,  $n_r$  is the real part of the refractive index, and  $n_i$  is the imaginary part of the refractive index which are determined by the real and imaginary parts of the complex susceptibility of the gain medium, and can be mathematically related using the Kramers-Kronig relation. Since the induced charges are very small compared to the refractive index, the expression is equivalent to:

$$a = \frac{dc_r/dN}{dc_i/dN} \quad (2.2)$$

Where  $c_r$  and  $c_i$  are the real and imaginary components of the complex susceptibility,

respectively.

Commonly the  $\alpha$ -parameter is described in the literature as<sup>8</sup>:

$$a = -\frac{4p}{l} \left( \frac{dn_r}{dN} \right) \left( \frac{dg}{dN} \right)^{-1} = -2k \left( \frac{dn_r}{dN} \right) \left( \frac{dg}{dN} \right)^{-1} \quad (2.3)$$

Where  $l$  is the wavelength,  $g$  is the optical gain, and  $k$  is the wave number. The refractive index can be calculated using the Kramers-Kronig relation:

$$n_r - 1 = \frac{ch}{2p^2} P \int_0^\infty \frac{-g(u)}{u^2 - E^2} du \quad (2.4)$$

where  $c$  is the speed of light,  $h$  is Plank's constant,  $P$  is the Cauchy principle value of the integral, and  $E$  is photon energy<sup>9</sup>. Using the former two equations, a general equation for the  $\alpha$ -parameter can be written as:

$$a = \frac{2E}{pg'(E)} P \int_0^\infty \frac{g'(u)}{u^2 - E^2} du \quad (2.5)$$

where  $g'$  is the differential gain.

## 2.4 Injection Locking Technique

When light from the master laser is injected into a multi-mode FP slave laser that is biased above threshold, the injected light competes with the optical gain of the slave, thereby significantly altering the slave's output beam. When this injected power is strong enough to create a significant injection ratio,  $h$ , a suppression of the side modes occurs. The ratio of the intensity of the peaks of the side modes relative to the locked mode is defined as the side mode suppression ratio (SMSR). Typically, the system is considered to be locked when a SMSR of 30 dB or greater is achieved on all of the modes, except for the one being locked, however this is not a strict rule, and is typically determined by the experimentalist. Figure 2.3 shows the free-running slave laser before injection (bottom) and a locked laser with a side modes suppressed beneath the noise floor creating an SMSR greater than 40 dB (top).

The measurement of the  $\alpha$ -parameter via an injection locking technique was first demonstrated and justified by Liu, Jin, & Chuang<sup>10</sup>. The major advantage this method has over the others listed above is that no fitting-parameters are required, reducing the uncertainty for different laser systems. This injection locking method takes advantage of the asymmetry in the stable locking region over a range of detuning on both the positive and negative side of the locked mode. The equation used to find the  $\alpha$ -parameter, and validated by Liu, Jin, and Chuang, under strong injection is<sup>10</sup>:

$$\frac{\Delta I_{pos}}{\Delta I_{neg}} = \sqrt{1 + a^2} \quad (2.6)$$

$$a = \sqrt{\left(\frac{\Delta I_{pos}}{\Delta I_{neg}}\right)^2 - 1}$$

Where  $DI_{pos}$  is the detuning difference when the master's wavelength is greater than the slave's, therefore on the positive, or red side, and  $DI_{neg}$  is the value when the master's wavelength is less than the slave's, hence on the negative, or blue side. The ratio of  $\frac{\Delta I_{pos}}{\Delta I_{neg}}$  should theoretically remain the same for any value of SMSR the observer chooses, therefore it should be chosen as large as the experiment will allow. In this way, the weak side modes of the slave laser that are next to the injection-locked mode are always observable above the noise floor.

In order to keep an accurate measurement, the minimum SMSR was kept at 35 dB for the reasons stated in the previous paragraph. It was also found that unless the modes were suppressed to below 35 dB relative to the peak of the regenerated signal; they can have a significant influence on the injection locking stability boundary, causing an unreliable measurement for the  $\alpha$ -parameter. This influence on the boundary has the effect of pulling the injection-locking detuning frequency towards the more dominate FP modes when locking on a weak side-mode.

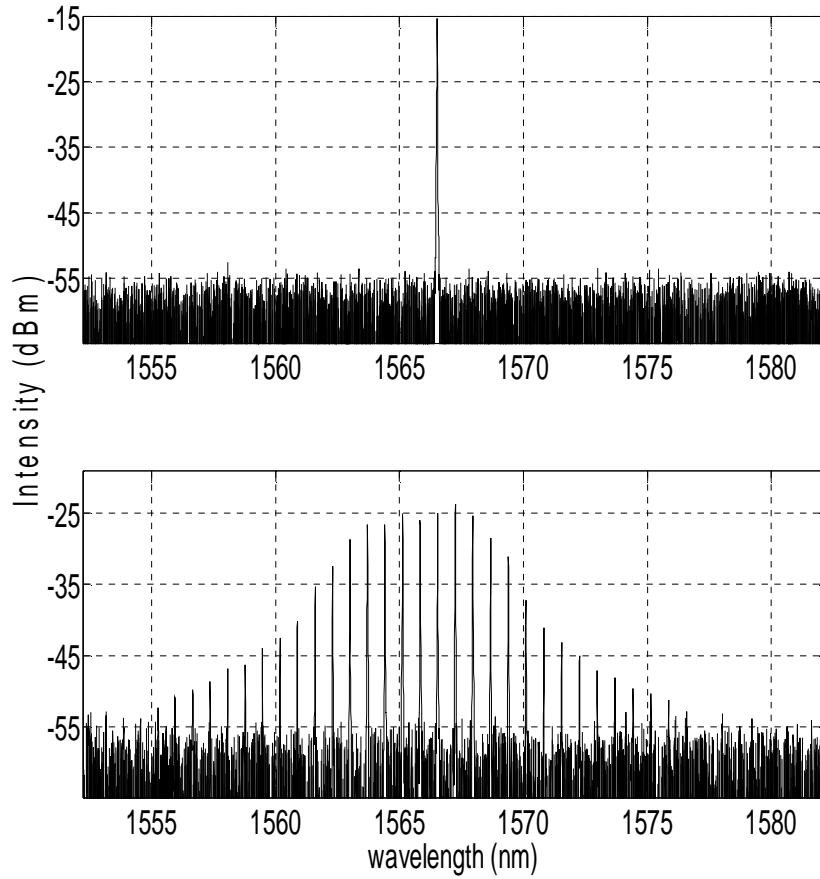


Figure 2.3) Optical spectra of the injection locked laser at a dominant FP mode (top) and the free-running slave (bottom) biased at 70 mA with a peak wavelength  $\sim 1567$  nm.

## 2.5 Wavelength and Power Dependence of the $\alpha$ -Parameter

When measuring the  $\alpha$ -parameter, it is also very important to know how it varies with both wavelength and injection power. Measuring the power dependence of the  $\alpha$ -parameter can be done two different ways: by varying the master power or by changing the slave power. The method described in section 2.4 to measure the linewidth enhancement-parameter was used for all three scenarios.

First, a measurement of the  $\alpha$ -parameter as a function of the injected power or photon density was performed, keeping a constant bias on the slave laser, and the wavelength a constant. This was easily done in the setup by one of three ways: adjusting the bias current (and thus the output power) of the master laser, adjusting the output power of the EDFA, or by tuning of the VOA. By varying the injected power into port 2 of the circulator from -12 dBm to 3 dBm,  $\eta=1.0*10^{-3}$  to  $7.2*10^{-2}$ , the  $\alpha$ -parameter stayed relatively constant from 1.0 to 1.3. In this locking range, the typical detuning values that were measured for  $\Delta\lambda_{\text{pos}}$  and  $\Delta\lambda_{\text{neg}}$  were on the order of 50 to 100 pm, with the resolution of the OSA being 20 pm. Thus, it is believed that the variation of the  $\alpha$ -parameter is a result of the resolution of the equipment when the asymmetry in the locking regime is small.

Second, a measurement of the  $\alpha$ -parameter as a function of the slave laser power was performed, keeping the master's power and wavelength constant. When the power was changed from 2.2 mW at a bias current 50 mA (5 mA above threshold) to 10.3 mW at a current of 100 mA (55 mA above threshold), the  $\alpha$ -parameter increased from 1.2 to 8.6, as shown in Fig. 2.4. This relatively large power dependence is related to the

nonlinear dynamics of the device, such as the nonlinear gain coefficient which will be discussed in Chapter 3. The  $\alpha$ -parameter follows the same general shape as the light intensity versus current (LI curve), including the saturation in the  $\alpha$ -parameter with the current that is caused by the thermal rollover of the device.

Lastly, a test of the dependence of the  $\alpha$ -parameter with wavelength was measured. This was done by keeping the master and slave's output powers constant, therefore creating a constant injection ratio, while tuning to different FP modes of the slave from very weak modes at 1550 nm, through the dominate FP modes at 1563 nm, to 1573 nm, the limitation of the band pass filter. The calculated value of the  $\alpha$ -parameter remained at 1.5 through the entire range, showing consistency in the data. This consistency through the entire range can be confirmed by performing an optical gain measurement using the Amplified Spontaneous Emission (ASE) technique.

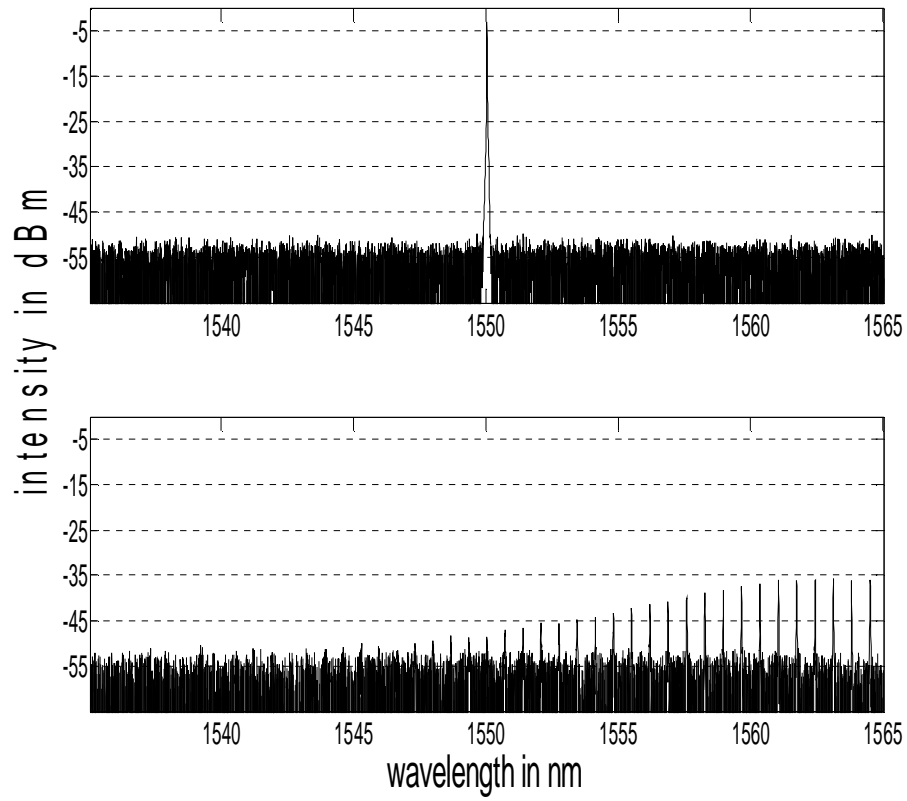


Figure 2.4) Optical spectra of the injection locked laser at a weak side mode at 1550 nm (top) and the free running slave (bottom) biased at 70 mA with a peak wavelength  $\sim$ 1565 nm.



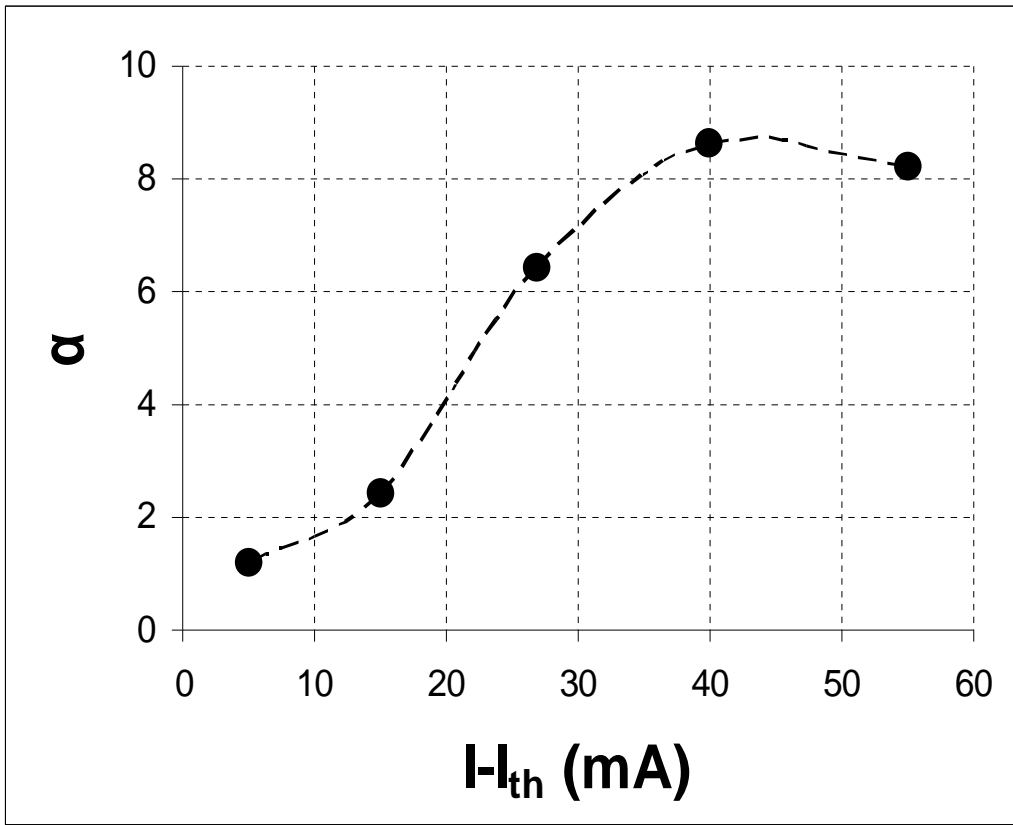


Figure 2.5) Plot of  $\alpha$  vs. current above threshold. The  $\alpha$ -parameter has a strong relation to the output power of the slave laser, indicating a large nonlinear gain coefficient.

## 2.6 ASE/Hakki Paoli Method for Determining Optical Gain

The amplified spontaneous emission (ASE) method of determining the optical gain, also known as the Hakki-Paoli Method, is the most common technique for measuring the  $\alpha$ -parameter. The method evaluates the net modal gain from the Fabry-Perot modulation depth (gain ripple) in the ASE spectra of an edge-emitting laser below threshold. Although this technique seems simple to perform, there are a few constraints to be aware of. First, it is only reasonable to measure the gain below threshold since the carrier density is clamped above threshold. Using an antireflection coating to lower the threshold increases the complexity of this method since the wavelength dependence of the facet reflectivity has to be known very accurately in order to evaluate the gain<sup>11</sup>. Also, this method requires the use of a high-resolution optical spectrum analyzer in order to reduce the error of the measurements.

An ASE spectra was obtained just below threshold at 44 mA using an Ando OSA with a resolution of 20 pm, using a point by point averaging of 100 scans, which took about 30 minutes to acquire. From the measured spectra, the net modal gain,  $g$ , can be extracted from the peak to valley ratio of the sub-threshold oscillations, shown in figure 2.6, using:

$$g = \frac{1}{L} \ln \left[ \frac{1 (\sqrt{x} - 1)}{r (\sqrt{x} + 1)} \right] \quad (2.7)$$

where  $L$  is cavity length  $x$  is the peak to valley power ratio, and  $r$  is the facet reflectivity.

Due to the noise in the valleys, as seen in figure 2.6, the gain can be underestimated by up to 10%.

Figure 2.7 is the resulting net modal gain of the InAs quantum dash laser. Over the range of 1550 nm to 1573 nm, the curve is relatively flat, indicating a small change in the gain over the entire region. The flatness of the net modal gain curve is directly related to the reason the  $\alpha$ -parameter remains fairly constant at 1.5 over this entire spectral range. Since there is little to no change in the gain or index of refraction over this region, the  $\alpha$ -parameter remains constant, as shown by equation 2.3.

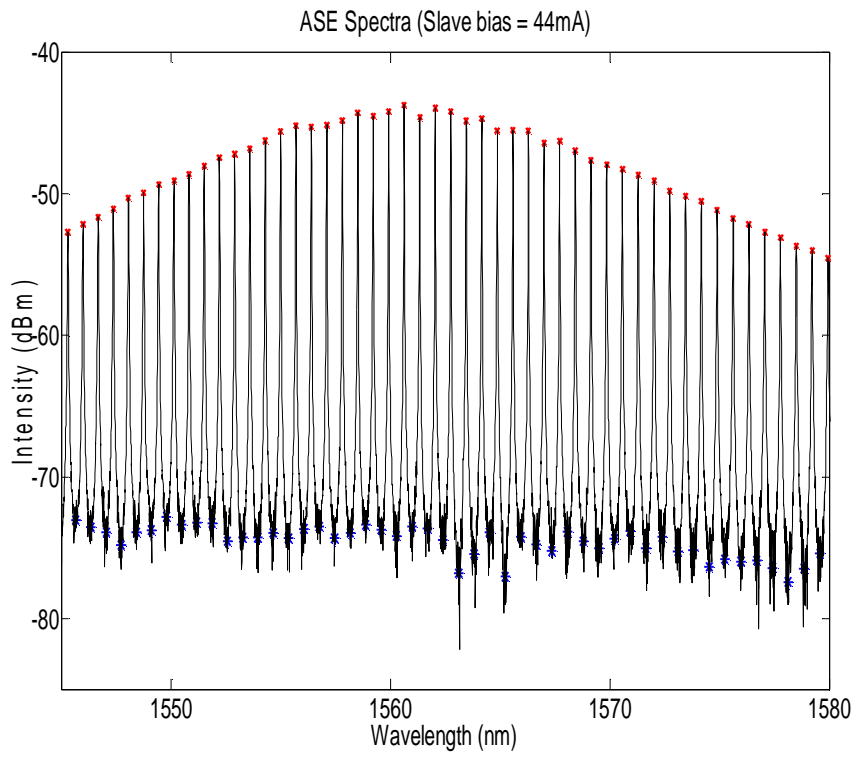


Figure 2.6) Measurement of the ASE at 44 mA (1 mA below threshold) showing the peaks marked in red, and valleys marked in blue.

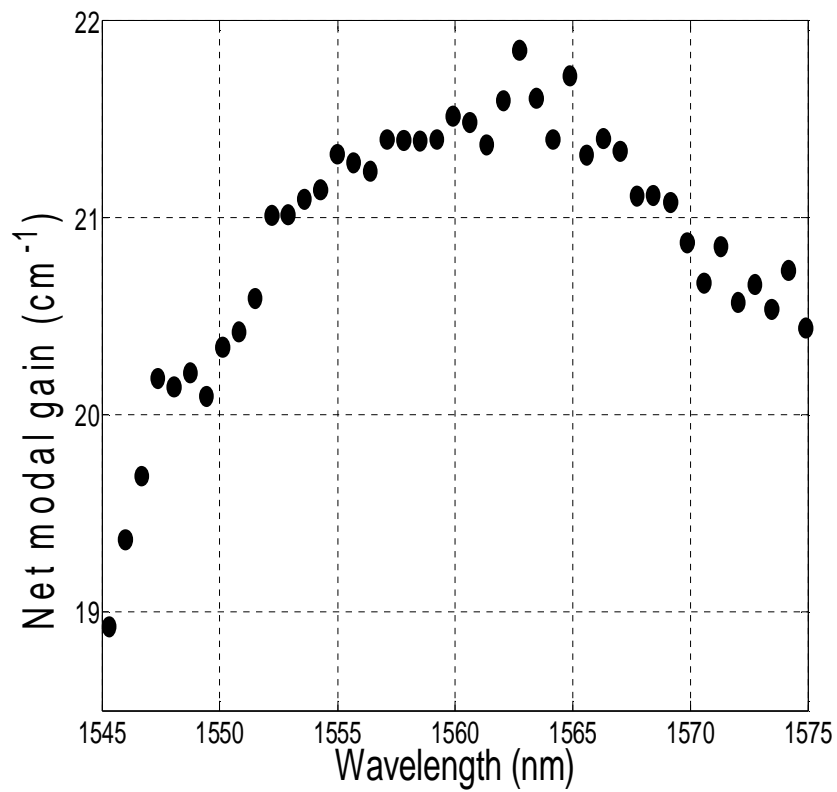


Figure 2.7) Net modal gain spectra calculated from the ASE spectrum. The relative flatness of the gain between 1550 nm and 1573 nm gives an indication of why the  $\alpha$ -parameter remained constant through the entire range.

## 2.7 Conclusion

In this chapter, the linewidth enhancement factor, its measurements, and results have been discussed. The device and experimental setup were described. For the first time, the  $\alpha$ -parameter of an InAs quantum dash laser was measured using an injection locking technique. The experimental setup used for the experiments allowed maximum control and resolution over the injection locking and detuning, respectively.

The  $\alpha$ -parameter was measured by varying the wavelength and by varying the injection ratio, both by tuning the master laser's power, and by tuning the slave laser's power. When the wavelength was changed all the way from 1550 nm to 1573 nm, the  $\alpha$ -parameter remained constant at 1.5 at a slave bias current of 60 mA. This was explained by the relatively flat gain curve over this region calculated from the ASE and Hakki-Paoli Method. The  $\alpha$ -parameter also remained constant when the power from the master laser was tuned from -12 dBm to 3 dBm, showing that the  $\alpha$ -parameter does not change with injected optical power into the slave cavity. Lastly, the  $\alpha$ -parameter was measured by varying the bias current of the slave laser. While changing the bias current, the  $\alpha$ -parameter varied from 1.2 to 8.6, following the general trend in the LI curve. The roll over of the  $\alpha$ -parameter at high currents was a result of the thermal rollover of the laser. A more detailed explanation of the dependence of the  $\alpha$ -parameter with the bias current will be discussed in Chapter 3.

## 2.7 References

---

- <sup>1</sup> Ehrhardt, J; Villeneuve, A; Stegeman, G.I; Nakajima, H; Landreau, J; Ougazzaden, A; "Interferometric measurement of the linewidth enhancement factor of a 1.55  $\mu\text{m}$  strained multi-quantum-well InGaAs/InGaAsP amplifier," IEEE Photonics Technology Letters, Vol. 4, pp. 1335-1338, 1992
- <sup>2</sup> Li, H; "RF-modulation measurement of linewidth enhancement factor and nonlinear gain of vertical-cavity surface-emitting lasers," IEEE Photonics Technology Letters, Vol. 8, pp. 1594-1596, 1996
- <sup>3</sup> Toffano, Z; Dextrez, A; Birocheau, C; Hassine, L; "New linewidth enhancement determination method in semiconductor lasers based on spectral analysis above and below threshold," Electronics Letters, Vol. 28, No. 1, pp 9-11, 1992
- <sup>4</sup> Barland, S; Spinicelli, P; Giacomelli, G; Marin, F; "Measurement of working-parameters of an air-post vertical-cavity surface emitting laser," IEEE Journal of Quantum Electronics, Vol. 41, No. 10, pp. 1235-1243, 1994
- <sup>5</sup> Kikuchi, K; "Lineshape measurement of semiconductor lasers below threshold," IEEE Journal of Quantum Electronics, Vol. 24, No. 9, pp 1814-1817, 1988
- <sup>6</sup> Newell, T.C; Bossert, D.J; Stintz, A; Fuchs, B; Malloy, K.J; Lester, L.F; "Gain and Linewidth Enhancement Factor in InAs Quantum-Dot Laser Diodes," IEEE Photonics Technology Letters, Vol. 11; No. 12; 1999
- <sup>7</sup> Fordell, T; Lindberg, A. M; "Experiments on the Linewidth-Enhancement factor of a Vertical-Cavity Surface-Emitting Laser," IEEE Journal of Quantum Electronics, Vol. 43, No. 1, 2007
- <sup>8</sup> Coldren, L.A; Corzine, S.W; "Diode Lasers and Photonic Integrated Circuits," John Wiley & Sons Inc, pp 207-213
- <sup>9</sup> Balanis, C.A; "Advanced Engineering Electromagnetics," John Wiley & Sons, Inc, pp. 72-85

---

<sup>10</sup> Liu, G; Jin, X; Chuang, S.L; “Measurement of Linewidth Enhancement Factor of Semiconductor Lasers Using an Injection-Locking Technique,” IEEE Photonics Technology Letters, Vol. 13, No. 5, 2001

<sup>11</sup> Gerhardt, N.C; Hofmann, M.R; “Experimental analysis of the optical gain and linewidth enhancement factor of GaInNAs/GaAs lasers;” Journal of Physics: Condensed Matter 16, 2004



### Chapter 3: Nonlinear Gain Coefficient and Operational Map

Since non-linear gain effects were first observed in semiconductor lasers, their influence on the dynamics and behavior of semiconductor lasers have been under investigation, but rarely in the context of injection locking<sup>1,2</sup>. The properties of injection-locking on a semiconductor laser have been studied since the early 1980's. A lot of effort has been made since then dealing with the locking range and stability, noise, modulation, chirp, linewidth reduction, microwave signal generation, and optical frequency conversion for applications in high-speed digital and coherent transmission systems<sup>3,4,5,6</sup>. However, very little research has been dedicated to the effect of non-linear gain on the injection-locking characteristics of a semiconductor-based slave laser. This chapter will examine in detail the extraction of the non-linear gain coefficient from injection-locking data and qualitatively describe the possible impact this parameter has on the injection locking characteristics.

The nonlinear gain coefficient is the measure of the suppression of the gain at high photon densities in a semiconductor laser and is most commonly attributed to spectral hole burning in a narrow bandwidth of the gain medium. Other causes include carrier heating and transport effects in the laser active region, but these phenomena do not strictly depend on the photon density, rather they are impacted by the statistical distribution of injected electrons and holes. In practical terms, the most serious detriment of the non-linear gain coefficient is to limit the modulation bandwidth of a semiconductor laser. As was alluded to in Chapter 2, the nonlinear gain coefficient can also effect the  $\alpha$ -

parameter above threshold, which as will be seen below allows us to calculate the nonlinear gain coefficient from this power dependence.

This chapter will also discuss the role that a widely varying  $\alpha$ -parameter could have on the injection-locking characteristics. For the purposes of analyzing the injection-locking behavior, it is common to use a so-called “operational map.” An operational map of an injection locking system is the detuning frequency versus injection ratio plot that illustrates the regions of different dynamical behaviors that the coupled master-slave system goes through. Lang<sup>7</sup>, in 1982, investigated the role of the linewidth enhancement factor in injection-locked devices, and showed that semiconductor lasers display unusual features such as asymmetry in their locking range, and a shift of coherence collapse around the point of the maximum power. In addition, large areas in the operation map exhibited unstable characteristics. Several studies have been performed to map out the different features of the injection-locked area with respect to detuning and injection ratio<sup>8, 9, 10</sup>. Therefore, the map serves as a diagnostic tool for comparing and understanding the behavior of the laser, as well as giving a better understanding of the effects that the linewidth enhancement factor and potentially the non-linear gain coefficient on the operation of the injection-locked laser.

### 3.1 Nonlinear Gain Coefficient

Nonlinear effects have a direct affect on the performance and operation of injection locked semiconductor lasers, especially those used for high-speed applications. Such effects, such as nonlinear gain saturation (or gain suppression), which is related to

the nonlinear gain coefficient can directly affect the modulation performance of these devices, and even dramatically change the  $\alpha$ -parameter and operational map of injection-locked semiconductor lasers. The suppression of the gain at high photon densities can be explained by several phenomena such as spatial hole burning, carrier heating, and two photon absorption<sup>11,12,13</sup>.

To account for the effects of the non-linear gain saturation, the power-related nonlinear gain coefficient,  $e_p$ , is introduced to modify the gain:

$$G \rightarrow \frac{G}{1 + e_p P} \quad (3.1)$$

where  $G$  is the gain of the laser active region and  $P$  is power output of the laser diode.

Introducing this term into the coupled rate equations, the new rate equations become:

$$\frac{dN}{dt} = \frac{I}{eV} - \frac{N}{t_{sp}} - \frac{G}{1 + e_p P} \quad (3.2)$$

$$\frac{dS}{dt} = \frac{\Gamma G S}{1 + e_p P} - \frac{S}{t_p} + \frac{bN}{t_{sp}} \quad (3.3)$$

Where  $I$  is the injected current,  $V$  is the volume of the optical gain medium,  $t_{sp}$  is the spontaneous carrier lifetime,  $N$  is carrier density,  $G$  is optical confinement factor,  $t_p$  is the photon lifetime in the cavity, and  $b$  represent the fraction of spontaneous emission that couples into the laser cavity mode. From the rate equations, it is evident that as the

power is increased, the gain becomes saturated at a rate proportional to the nonlinear gain coefficient. For a large nonlinear gain coefficient,  $e_p$ , the gain is saturated at a faster rate and this is deleterious to the modulation bandwidth.

### 3.2 Relation Between the Nonlinear Gain Coefficient and $\alpha$ -Parameter

Taking the rate equations further, the relationship between the power,  $P$ , and frequency chirp,  $Dn$ , can be expressed using the equations:

$$\frac{dS}{dt} = \left( \frac{\Gamma v_g g}{1 + e_p P} - G_{th} \right) P + R_{sp} \quad (3.4)$$

$$\Delta u = u - u_{th} = -\frac{u_{th}}{n} \Delta n = -\frac{u_{th}}{n} \frac{\partial n}{\partial g} (g - g_{th}) = \frac{a}{4p} \Gamma v_g (g - g_{th}) = \frac{a}{4p} (\Gamma v_g g - G_{th}) \quad (3.5)$$

However, frequency chirp can be manipulated further and be expressed as:

$$\begin{aligned} \Delta u &\approx \frac{a}{4p} \left[ (1 + e_p P) \frac{dP}{P dt} + e_p P G_{th} \right] \\ &= \frac{a}{4p} (1 + e_p P) \left[ \frac{dP}{P dt} + \frac{e_p P G_{th}}{(1 + e_p P)} \right] \\ &= \frac{a_{eff}}{4p} \left[ \frac{dP}{P dt} + \frac{e_p P G_{th}}{(1 + e_p P)} \right] \end{aligned} \quad (3.6)$$

where  $a_{eff}$  is the effective  $\alpha$ -parameter,  $P$  is the optical power,  $t$  is time,  $e_p$  is the power

nonlinear gain coefficient,  $G$  is material gain,  $v_g$  is the group velocity, and  $G_{th}$  the threshold gain of the laser<sup>14</sup>. Thus, equation 3.6 shows how the frequency chirp depends on the  $\alpha$ -parameter and motivates how we expect the actual measured, effective  $\alpha$ -parameter to vary linearly with output power, i.e.,

$$a_{eff} = a_0(1 + e_p P) \quad (3.7)$$

### 3.3 Calculation of the Nonlinear Gain Coefficient

As described in the previous section, the  $\alpha$ -parameter is a function of the power. By knowing this relationship, the nonlinear gain coefficient can be extracted. Chapter 2 described how the  $\alpha$ -parameter changes with current above threshold, or more specifically the power above threshold. By measuring a light vs. current (LI) curve, the  $\alpha$ -parameter vs. power curve can be created as shown in Figure 3.1.

A curve fit using equation (3.7) can be applied to this graph to extract  $e_p$ , as shown in Figure 3.1. The  $\alpha$ -parameter of the InAs/AlGaInAs quantum dash laser was measured to be 1.2 at 2 mW output power and increased to 8.6 at an output power of 10.2, leading to an  $e_p = 0.7 \text{ mW}^{-1}$ . The nonlinear gain coefficient, which is normally defined in terms of the photon density, is related to  $e_p$  by:

$$e_s S = e_p P \quad (3.8)$$

Where  $e_s$  is the nonlinear gain coefficient and  $S$  is the photon density.  $S$  is considered to be constant through the entire cavity length, therefore it can be calculated by:

$$S = \frac{P}{E_{ph} v_g \ln\left(\frac{1}{R}\right) A_m} \quad (3.9)$$

Where  $E_{ph}$  is the photon energy,  $v_g$  is the group velocity,  $R$  is the power reflectivity of the facet (assumed to be the same for both facets), and  $A_m$  is the near-field area of the mode calculated by  $width * \frac{height}{\Gamma}$ , which is approximately  $1.6 \mu\text{m}^2$ .

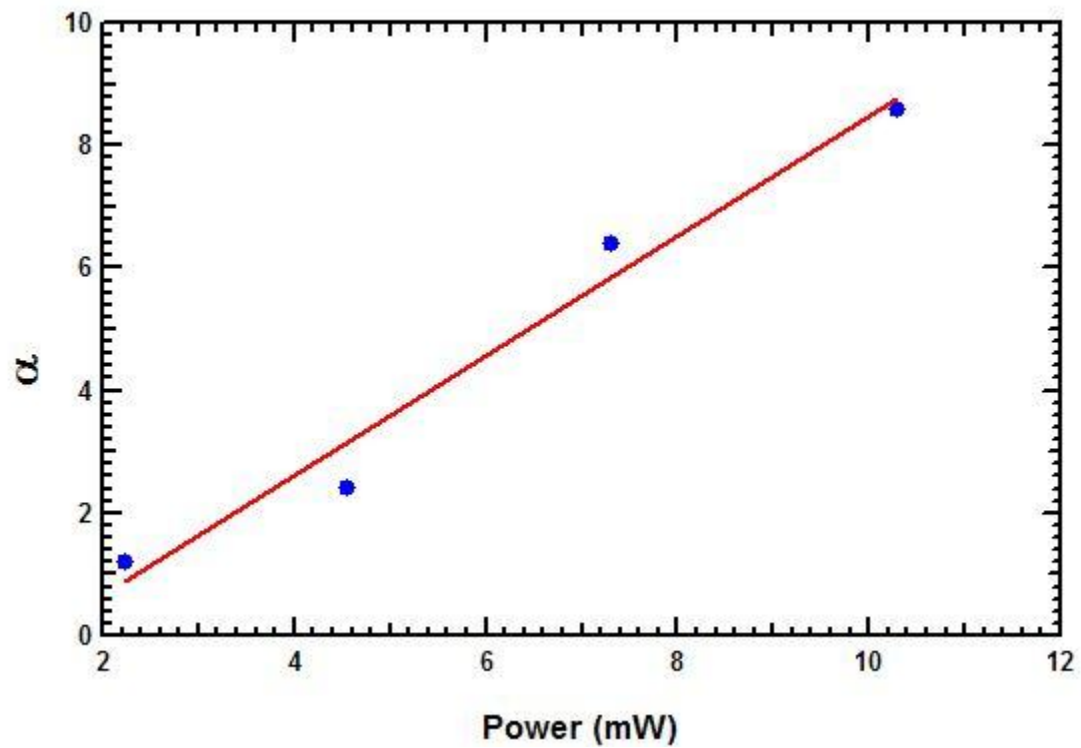


Figure 3.1. The  $\alpha$ -parameter vs. output power of the slave laser. The blue dots represent the measured data points. A strong dependence on power is noticeable. The red line is a curve fit of  $\alpha$  vs. power.

From the data, the value of  $e_s$  for the InAs quantum dash laser was calculated to be  $1.4 \times 10^{-14} \text{ cm}^3$ , 100 times larger than the previously reported values for quantum dots of  $1.6 \times 10^{-16} \text{ cm}^3$ <sup>14</sup> and 1000 times larger than typical quantum well devices.<sup>15</sup> Typically, large  $e_s$  is an unwanted feature for applications such as high speed lasers due to the large saturation of gain with power. However, this huge increase in the nonlinear gain coefficient changes many of the dynamic properties of the laser, such as shifting the operational map, and preventing such features as coherence collapse. This impact on the operational map of an injection-locked quantum dash laser is analyzed in the next section.

### 3.4 Experimental Apparatus for Generating the Operational Map

The InAs quantum dash device described in section 2.1 was used for this experiment. The fiber-based optical injection set-up using a three port circulator as described in section 2.2 was implemented again with the addition of an Agilent 83453B Technologies High Resolution Spectrometer (HRS). The HRS has a resolution of 1 MHz has a relatively wide frequency scan range and fast acquisition times. Spectra were taken at a detuning step interval of 1 GHz, except for transitional stages, where the spectra were taken in smaller intervals. To determine whether the system was locked, constant monitoring of the SMSR was kept track of using the second optical spectrum analyzer.

The Agilent 83453B HRS uses a heterodyne technique to detect and measure optical signals from 1440 nm to 1640 nm. A signal from the injection locking system is mixed with a swept local oscillator, an Agilent tunable laser, inside of a balanced receiver. The design allows the separation of the usable coherent light and a common mode of the



signal. By subtracting the currents generated in the balanced receiver, the common mode, direct detection components are reduced relative to the desired heterodyne signal. This common mode rejection reduces noise and improves the dynamic range. Polarization independence is improved by depolarizing the local oscillator<sup>16</sup>.

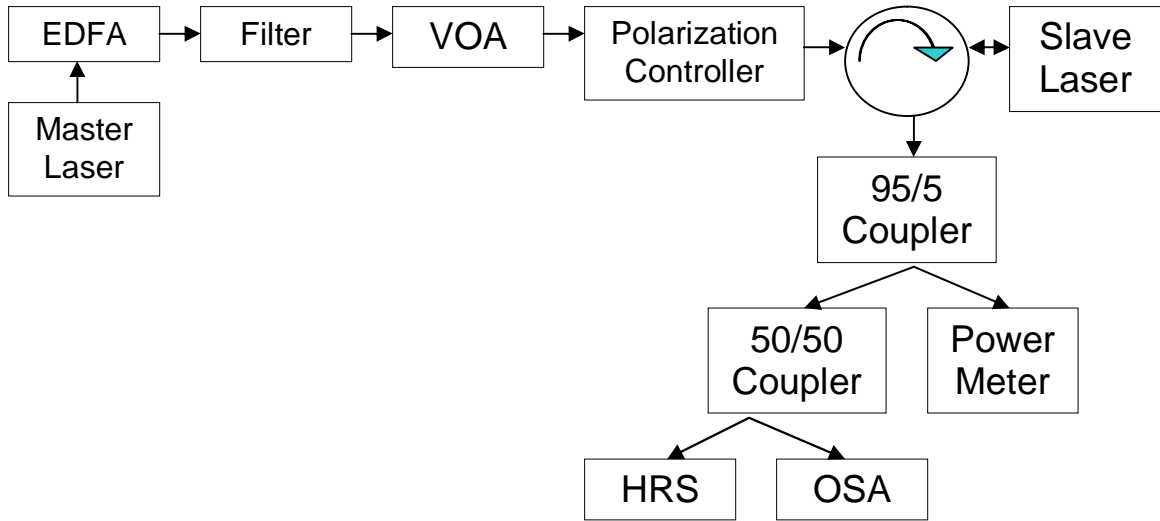


Figure 3.2: Schematic of the experimental setup used for measuring the operational map. The addition of the HRS allows for very fine measurements, with a resolution as low as 1 MHz where needed.

### 3.5 Measuring the Operational Map of the InAs Quantum Dash Injection-Locked Laser

An operational map was created, shown in Figure 3.3, using the experimental setup described above. To plot the map, detailed scans of the spectrum were studied, and the transitional points from state to state were recorded. The roughness of the map comes from having a resolution of 15 MHz, and the fact that the transitions were not instantaneous. Typically, a small range of 10s of MHz was needed to completely go from one state to the next.

The map was created using an InAs QDash device as the slave laser and has a few advantages not recorded in previous maps of injection-locked semiconductor lasers. In a side-by-side comparison of our operational map created with the InAs QDash laser used in this experiment and a conventional edge-emitting laser used by Simpson, Liu, Huang, and Tai, we can note many interesting changes. First, a region of stable locking is present over the entire range of injection ratios on the positive detuning side of the map. Second, and most importantly, is that at zero detuning, the system goes from stable locking, to period one, and eventually back to stable locking again. This has positive implications for optical networks in that an optical isolator is not needed in laser transmitter packages since any amount of optical feedback will not make the system go into a period doubling or unstable coherence collapse. At present, our understanding is that the operational map's properties are largely determined by the  $\alpha$ -parameter and the nonlinear gain coefficient. Since the InAs QDash lasers have a lower  $\alpha$ -parameter and a giant nonlinear gain coefficient compared to conventional quantum well lasers, the

operational map takes on a much different form than a map of other lasers. The detailed theoretical study of this interesting combination of  $a$  and  $e_s$  is left to future research.

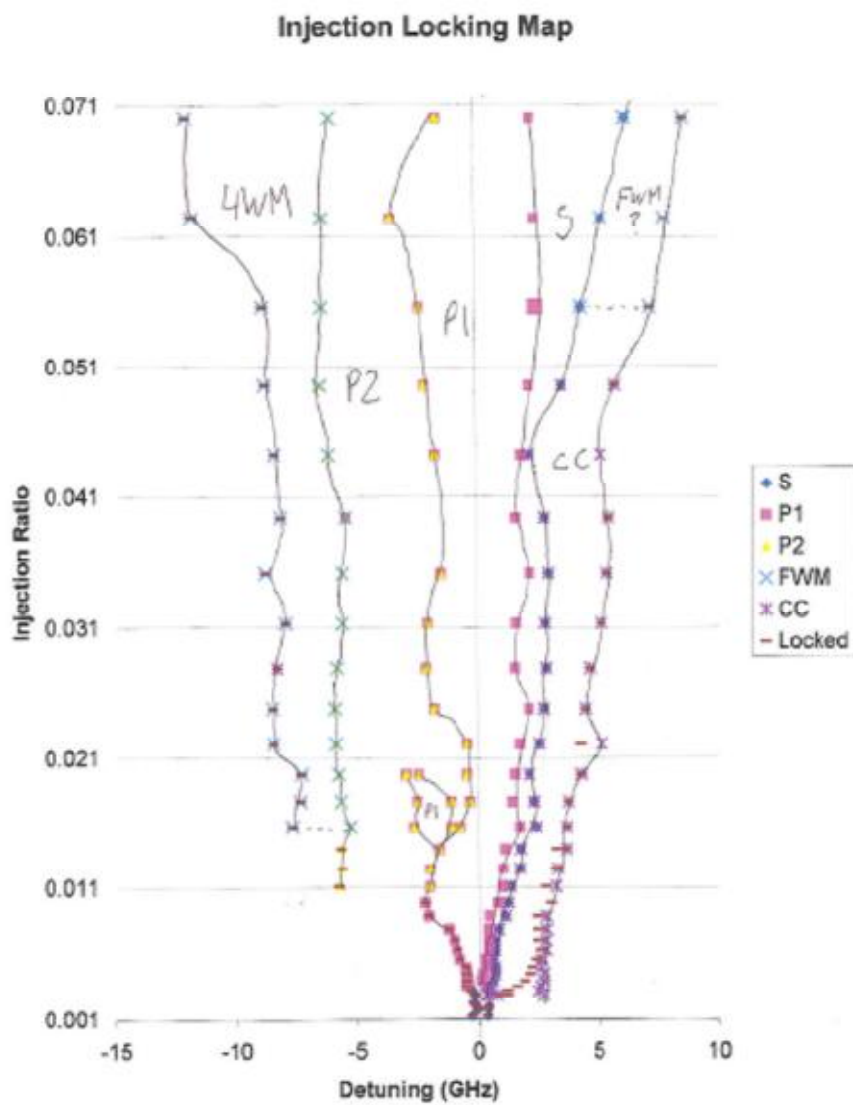


Figure 3.3. Operational map of an InAs Quantum Dash injection-locked laser. The shape of the map, influenced by the nonlinear gain coefficient and the  $\alpha$ -parameter, remains in a stable state and does not experience any coherence collapse for any level of injection at zero detuning. The bias on the slave laser was set at 60 mA, which corresponds to an  $\alpha$  of roughly 2.

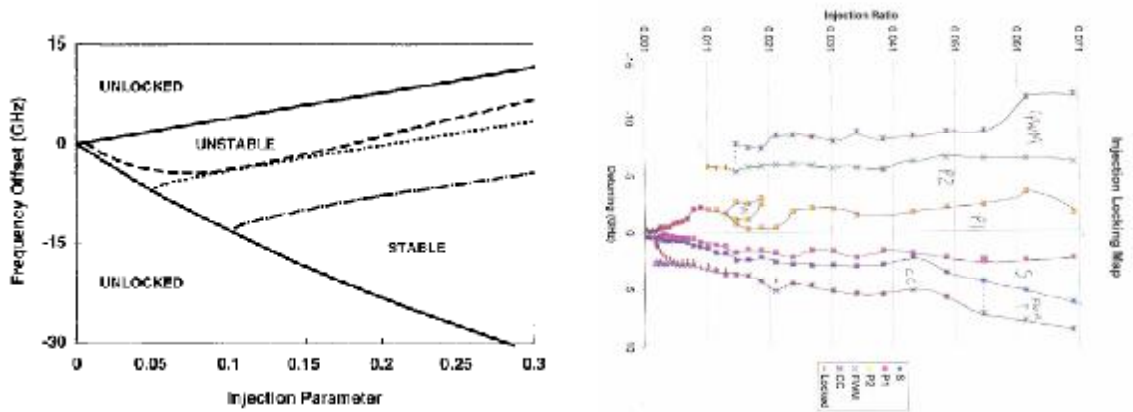


Figure 3.4. A side-by-side comparison of an operational map from a conventional edge-emitting semiconductor laser (left) and an InAs quantum dash edge-emitting laser (right). Since the InAs quantum dash laser has a lower  $\alpha$ -parameter and larger  $e_s$ , the map has shifted, and a coherence collapse region does not occur for the InAs quantum dash laser at 0 detuning, as it does for the conventional edge-emitting semiconductor laser.

### 3.6 Spectral Characteristics of the Different States in the Operational Map

Under injection-locking conditions, the system can be in one of six states: unlocked, stably-locked, period one, period doubling, four-wave mixing, or coherence collapse.

#### *Unlocked*

When the frequency between the master and the slave is large enough, the two beams are completely separated in an unlocked state. In this condition, the master's and slave's beams are completely unmixed, as shown in Figure 3.6a.

#### *Stable Locking*

Figure 3.6b shows a single sharp line at the injection frequency. This condition is known as the stable locking condition. When the master's light is injected into the multi-mode slave laser's cavity, the beam is regenerated, creating a single, sharp output with narrow linewidth, low chirp, and low noise.

#### *Period One*

The presence of relaxation oscillation sidebands is shown in Figure 3.6c. As the laser is turned on, the photon populations build up rapidly, thereby reducing the carrier density until it falls below the steady state value, making the stimulated recombination rate very small. As the carrier density begins to build up again, from a higher initial value, the photon population follows, resulting in a damped oscillatory optical output<sup>17</sup>.

The relaxation oscillations are a beneficial effect. The value of the relaxation oscillation frequency is very similar to the frequency where resonance occurs; therefore a large relaxation is required to create a large resonance frequency and large modulation bandwidth.

### ***Period Doubling***

As seen in previous research over the past few years, the onset of period doubling is a route to chaotic behavior. The onset of period doubling manifests itself as that of a parametric oscillator in that region, where the resonance frequency,  $w_r$ , and damping rate,  $g$ , of the oscillator are time dependent. If the resonance frequency varies at roughly twice the natural frequency of the oscillator, the oscillator becomes phase-locked to the parametric variation, and absorbs energy at twice the rate as it already had. In the regime of period doubling, the system can be described by:

$$\frac{d^2x(t)}{dt^2} + g(t)\frac{dx}{dt} + w_r^2(t)x(t) = 0 \quad (3.10)$$

This equation is linear in  $x(t)$ . The parameters  $w_r^2$  and  $g$  depend only on time and do not depend on the state of the oscillator. Therefore, they are typically assumed to vary periodically with period T.

### ***Four Wave Mixing***

Four-wave mixing is a non-linear effect arising from a third-order optical



nonlinearity. It can occur if at least two different frequency components propagate together in a nonlinear medium such as in the slave cavity. The master and slave frequencies  $f_m$  and  $f_s$  obtain a refractive index modulation at a difference frequency, which creates sidebands for each of the input waves. This effect creates two new frequency components<sup>18</sup>:

$$f_3 = 2f_m - f_s \quad (3.11)$$

$$f_4 = 2f_s - f_m \quad (3.12)$$

Figure 3.6e. shows the FP slave mode and the narrow master laser mode, as in the unlocked case, however with two extra peaks that arise from the four-wave mixing.

### ***Coherence Collapse***

An important, yet usually undesirable characteristic, of injection locked lasers is the onset of coherence collapse. Coherence collapse, which is a sudden broadening of the linewidth up to  $\sim 10$  GHz<sup>19</sup> caused by optical feedback or injection as shown in Figure 3.6f, can cause havoc if not addressed in an optical network that uses semiconductor laser transmitters. The technological solution in the past has been to place an optical isolator into the transmitter laser package, at the expense of adding size and cost. There has been considerable effort in order to reduce or eliminate the effect of coherence collapse<sup>20,21</sup>.

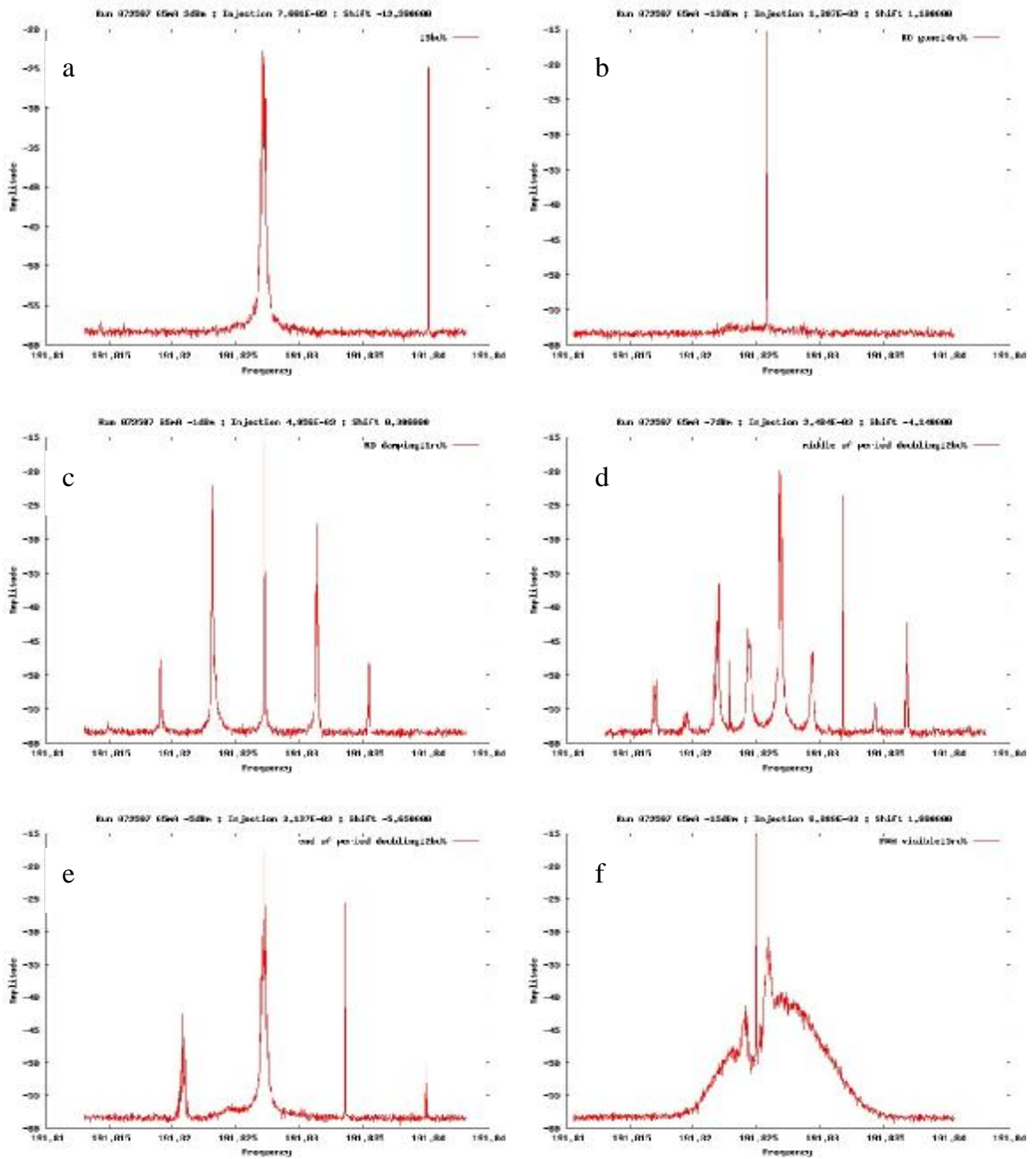


Figure 3.5: Spectrum of a) Unlocked, b) Stable Locked, c) Period 1 d) Period Doubling, e) Four Wave Mixing, f) Coherence Collapse

### 3.7 Zero Detuning

As noted before, at zero detuning, the InAs quantum dash laser only goes from stable locking, to period one, and back to stable locking, completely avoiding any unstable or unwanted states such as four-wave mixing, period doubling, and especially coherence collapse. The result of this stability at zero detuning leads to cheaper, smaller packaging for laser transmitters as there is no need for any optical isolators.

The relaxation oscillations in the period one region of the map were observed to increase from 3.9 GHz at low injection ratios to 5.3 GHz at high injection ratios. Characteristic data are shown in Fig. 3.7. The resonance frequency of the injection-locked coupled master-slave system can be expressed as<sup>22</sup>:

$$f_r = \frac{1}{2p} \sqrt{\frac{1}{t_p} \frac{g_{fr} g_M}{(g_{fr} + g_M)}} \quad (3.13)$$

where:

$$g_M = \frac{c}{2n_r L} \sqrt{h} (\cos f - a \sin f) \quad (3.14)$$

where  $t_p$  is the photon density,  $g_{fr}$  and  $g_M$  are the damping rates associated with free running and the master lasers,  $c$  is the speed of light,  $n_r$  is the group refractive index,  $L$  is the cavity length,  $h$  is the power injection ratio, and  $f$  is the phase difference between the master and slave. For a constant slave damping rate, increasing the injection ratio increases  $g_M$  which then increases the resonance frequency as shown in equation 3.13.

Each spectrum has small peaks at +/- 3.9 GHz that are caused by parasitic

feedback of the slave power from either the lensed fiber or the circulator. Since the slave power is not changed, this explains why these peaks are present in each spectrum and don't vary in position.

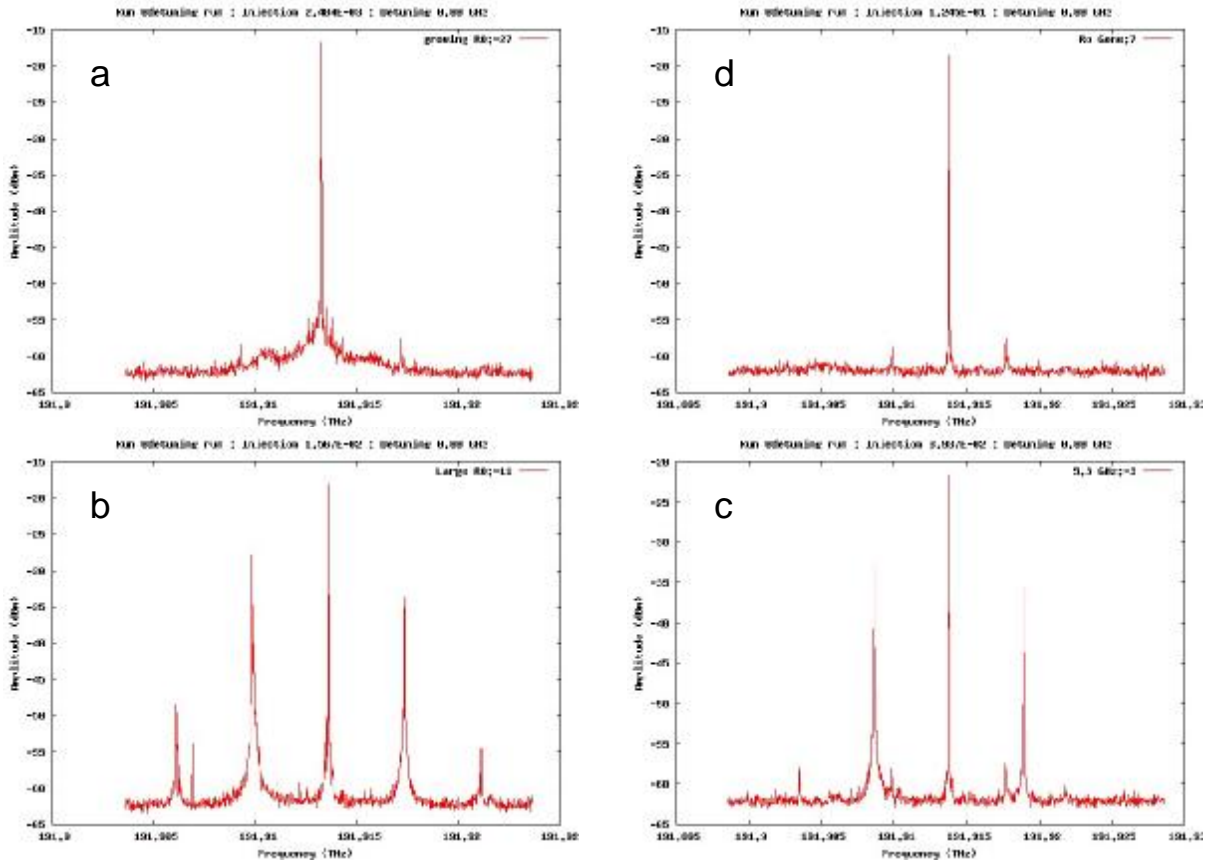


Figure 3.6. Spectra of InAs quantum dash laser injection-locked with zero detuning and a)  $\eta=2.48 \times 10^{-3}$  and no relaxation oscillations, b)  $\eta=1.57 \times 10^{-2}$  and relaxation oscillations 3.9 GHz apart, c)  $\eta=3.94 \times 10^{-2}$  and relaxation oscillations 5.3 GHz apart, d)  $\eta=1.245 \times 10^{-1}$  and no relaxation oscillations

### 3.8 Conclusion

In this chapter, we discussed the importance of gain saturation and the nonlinear gain coefficient, along with the related effects that may have possible influences on the dynamics of the semiconductor laser. It was found that the nonlinear gain coefficient is the contributing factor that increases the linewidth enhancement-factor with power. By doing a simple curve fit on the  $\alpha$ -parameter versus power, a nonlinear gain coefficient of  $1.4 \times 10^{-14} \text{ cm}^3$  was obtained, which is two orders of magnitude than the value previously reported for quantum dot materials, and three orders or magnitude larger than the value reported for a typical quantum well laser.

Next, with the help of an Agilent Technologies High Resolution Spectrometer, an operation map was created in order to observe the effect of a giant nonlinear gain coefficient and a small  $\alpha$ -parameter had on the injection-locked InAs quantum dash slave laser. It was found that the giant nonlinear gain coefficient and small  $\alpha$ -parameter had a shifting affect on the map over previously measured operational maps of different devices. This shift has many beneficial attributes, such as a completely stable region at 0 detuning, for an entire range of injection levels, thereby eliminating the need for costly optical isolators in coherent communication transition packages.

From the operational map, it was found that the system can be in any of six unique states: unlocked, stable locking, period one with relaxation oscillations, period two or period doubling, four wave mixing, and coherence collapse. It was found that period one is a beneficial state to improve modulation bandwidth. The relaxation oscillations are a function of injected photon density, being able to go from a limit of 3.9 GHz, the resonance frequency of the free running slave, to 5.3 GHz.

## 3.9 References

- 
- <sup>1</sup> Chrostowski, L; "Optical Injection Locking of Vertical Cavity Surface Emitting Lasers," University of California at Berkeley, 2003
- <sup>2</sup> Jin, X; Chuang, S.L; "Relative intensity noise characteristics of injection-locked semiconductor lasers," *Applied Physics Letters*, Vol. 77, No. 9, 2000
- <sup>3</sup> S. Mohrdiek, H. Burkhard, and H. Walter, "Chirp reduction of directly modulated semiconductor lasers at 10 Gb/s by strong CW light injection," *J. Lightw. Technol.*, vol. 12, no. 3, pp. 418-424, Mar. 1994
- <sup>4</sup> J. Wang, M. K. Haldar, L. Li, and F. V. C. Mendis, "Enhancement of modulation bandwidth of laser diodes by injection locking," *IEEE Photon. Technol. Lett.*, vol. 8, no. 1, pp. 34-36, Jan. 1996
- <sup>5</sup> T. B. Simpson, J. M. Liu, K. F. Huang, K. Tai, C. M. Clayton, A. Gavrielides, and V. Kovanis, "Cavity enhancement of resonant frequencies in semiconductor lasers subject to optical injection," *Phys. Rev. A*, vol. 52, no. 6, pp. R4348-51, Dec. 1995
- <sup>6</sup> X. J. Meng, T. Chau, and M. C. Wu, "Improved intrinsic dynamic distortions in directly modulated semiconductor lasers by optical injection locking," *IEEE Trans. Microwave Theory Tech.*, vol. 47, no. 7, pp. 1172-1176, Jul. 1999
- <sup>7</sup> Lang, R; "Injection locking properties of a semiconductor laser," *IEEE Journal of Quantum Electronics*, Vol. 18, No. 6, 1982
- <sup>8</sup> Kovanis, V; Gavrielides, A; Simpson, T.B; Liu, J.M; "Instabilities and chaos in optically injected semiconductor lasers," *Applied Physics Letters*, Vol. 67, No. 19, 1995
- <sup>9</sup> Simpson, T.B; "Mapping the nonlinear dynamics of a distributed feedback semiconductor laser subject to external optical injection," *Optics Communications*, 215, 2003
- <sup>10</sup> Troger, J; Nicati, P.A; Thevenaz, L; Robers, Ph. A; "Novel Measurement Scheme for Injection-Locked Experiments," *IEEE Journal of Quantum Electronics*, Vol. 35, No. 1, 1999
- <sup>11</sup> Agrawal, G.P; "Gain nonlinearities in semiconductor lasers: Theory and application to distributed feedback lasers," *IEEE Journal of Quantum Electronics*, Vol. 23, 1987
- <sup>12</sup> Agrawal, G.P; "Effect of gain and index nonlinearities on single-mode dynamics in semiconductor lasers," *IEEE Journal of Quantum Electronics*, Vol. 26, 1990
- <sup>13</sup> Channin, D.J; "Effect of gain saturation on injection laser swithing," *J Applied Physics Letters*, Vol. 50, 1979
- <sup>14</sup> Su, H; Zhang, L; Gray, A.L; Wang, R; Varangis, P.M; Lester, L.F; "Gain compression coefficient and above-threshold linewidth enhancement factor in InAs/GaAs quantum dot DFB lasers," *Physics and Simulation of Optoelectronic Devices XIII*, Proc. of SPIE Vol. 5722
- <sup>15</sup> Girardin, F; Duan, G.H; Gallion, P; Talneau, A; Ougazzaden, A; "Experimental investigation of the relative importance of carrier heating and spectral hole burning on nonlinear gain in bulk and strained multi-quantum-well 1.55  $\mu\text{m}$  lasers," *Applied Physics Letters*, Vol. 67, No. 6, 1995

---

<sup>16</sup> Agilent Technologies, “Agilent 83453B High-Resolution Spectrometer; Technical Specifications,” <http://cp.literature.agilent.com/litweb/pdf/5988-5309EN.pdf>, 2005

<sup>17</sup> Bhattacharya, P; “Semiconductor Optoelectronic Devices, Second Edition,” Prentice Hall, 1997, Chapter 7, pg. 322 – 325

<sup>18</sup> Thiel, C.W; “Four-wave mixing and its applications,” <http://www.physics.montana.edu/students/thiel/docs/FWMixing.pdf>

<sup>19</sup> Li, H; Ye, J; McInerney, J.G; “Detailed Analysis of Coherence Collapse in Semiconductor Lasers,” IEEE Journal of Quantum Electronics, Vol. 29, No. 9, 1993

<sup>20</sup> Petermann, K; “External Optical Feedback Phenomena in Semiconductor Lasers,” IEEE Journal of Selected Topics in Quantum Electronics, Vol. 1, No. 2, 1995

<sup>22</sup> Li, Y; Naderi, N.A; Kovanis, V; Lester, L.F; “Modulation Response of an Injection-Locked 1550 nm Quantum Dash Semiconductor Laser,” LEOS Annual Meeting, Orlando, FL, 2007



## Chapter 4: Concluding Remarks and Future Work

### 4.1 Concluding Remarks

This thesis presented injection locking characteristics of Indium Arsenide (InAs) quantum dash (QDash) lasers. Topics such as the linewidth enhancement factor ( $\alpha$ -parameter), nonlinear gain coefficient, and an operational map were discussed, measurements techniques, and results were discussed.

Chapter one started with a discussion of injection locking, and gave a brief introduction to the injection locking technique, master lasers, slave lasers, and important parameters such as frequency detuning and injection ratio. Applications using the injection locking technique, such as radio over fiber (ROF), millimeter wave generation, and all-optical signal processing were discussed. Chapter one also gave a discussion of quantum dashes, how they are formed and their advantages over bulk and quantum well materials, such as: large characteristic temperatures, low threshold current, small linewidth enhancement factor, and resistance to optical feedback.

Chapter two was dedicated to the measurement of the  $\alpha$ -parameter using the injection technique, device structure of the InAs QDash slave laser, and the experimental setup. The  $\alpha$ -parameter was measured using the asymmetries in the locking region.

The  $\alpha$ -parameter was measured as functions of injected photon density, wavelength, and output power of the slave laser. By keeping the wavelength and laser bias on the slave constants, the  $\alpha$ -parameter was found to be a constant function of the injected photon density, staying at  $\sim 1.3$ . The  $\alpha$ -parameter was also found not to change

between 1550 nm to 1573 nm. The Hakki-Paoli method, a technique that utilized the below threshold amplified spontaneous emission spectrum, was used to measure the modal gain in this region. The gain spectrum was found change less than 5% over the region, indicating a possible reason for the constant  $\alpha$ -parameter. A measurement of the  $\alpha$ -parameter as a function of the slave's output power resulted in a change from 1.2 to 8.4 showing a large dependence on the output power. The plot of the  $\alpha$ -parameter versus the injected current about threshold is shown in figure 2.5. Such a significant change in the  $\alpha$ -parameter versus power indicates a large nonlinear gain coefficient.

Chapter three presented the nonlinear gain measurement, its relationship to the  $\alpha$ -parameter, as well as the operational map of the injection locked InAs QDash laser. The nonlinear gain coefficient was found using a curve fit of  $\alpha$  versus power curve. The power nonlinear gain coefficient was found to be  $0.7 \text{ mW}^{-1}$ , which corresponds to a nonlinear gain coefficient of  $1.4 * 10^{-14} \text{ cm}^3$ . The value found is  $\sim 1000$  times larger than that of a typical quantum well semiconductor laser, and 100 times larger than previously reported within our own group of quantum dot semiconductor lasers.

Although a large nonlinear gain coefficient is not a favorable parameter for high speed applications, it can alter the operational map of the laser, preventing coherence collapse at zero detuning, an unstable region where the linewidth can increase to  $\sim 10$ s of GHz. To create the operational map of the InAs QDash laser, an Agilent Technologies High Resolution Spectrometer (HRS), with a resolution of 1 MHz was used. The use of such a high resolution spectrometer allowed us to see six unique operational states, unlocked, stable locking, period one where relaxation oscillations are present, period two

or period doubling, four wave mixing, and coherence collapse. By making the transition point on a detuning versus injection ratio graph, we were able to map out the operational behavior of the laser, which is mainly determined by the  $\alpha$ -parameter and nonlinear gain coefficient. With such a low  $\alpha$ -parameter and large nonlinear gain coefficient of the InAs QDash laser, the map looked much different than others previously recorded for different types of devices. The map was found to have shifted, only going from stable locking to period one, and back to stable locking, completely preventing coherence collapse, four wave mixing, and period doubling happening for any amount of optical feedback fed back into the cavity. The implications of this result in less bulky and lower cost optical transmitters for coherent communication systems since the optical isolator can be eliminated.

## 4.2 Future Work

The exciting results found within this thesis have created many additional ideas and questions to be answered. Currently, studies to increase the bandwidth by changing the detuning and injection ratio are being done in our group. To do this, the slave laser is biased at a high current, so that the  $\alpha$ -parameter becomes as large as 6 or 8 as demonstrated in chapter 2. When this is done, the detuning range will also increase, theoretically increasing the bandwidth. Work is also being done within our group if optimizing an injection locking setup for 1.3  $\mu\text{m}$  experiments. Once the experimental setup is done, work on 1.3  $\mu\text{m}$  InAs quantum dot will be performed, similar to that done on the 1.55  $\mu\text{m}$  quantum dash lasers. Also, we would like to replace the FP slave laser

with a DFB laser since DFB lasers inherently have a larger bandwidth than FP lasers. This will hopefully allow us to push the bandwidth even further. Other work being done currently is mathematical and computer aided modeling of these systems to give a better understanding of the underlying physics of the injection locked system.